Synthesis, spectral characterization, molecular modeling, antibacterial and antioxidant activities and stability study of binuclear Pd(II) and Ru(III) complexes with novel bis-[1-(2-[(2-hydroxynaphthalen-1-yl)methylidene]amino ethyl)-1-ethyl-3-phenylthiourea] ligand Application to detection of cholesterol

Achour Terbouche, Chafia Ait-Ramdane-Terbouche, Zineb Bendjilali, Hafida Berriah, Houria Lakhdari, Djahida Lerari, Khaldoun Bachari, Djillali Mezaoui, Nour El Houda Bensiradj, Jean-Paul Guégan, et al.

Synthesis, spectral characterization, molecular modeling, antibacterial and antioxidant activities and stability study of binuclear Pd(II) and Ru(III) complexes with novel bis-[1-(2-[(2-hydroxynaphthalen-1-yl)methylidene]amino}ethyl)-1-ethyl-3-phenylthiourea] ligand: application to detection of cholesterol.

Achour TERBOUCHE[a, *], Chafia AIT-RAMDANE-TERBOUCHE[a], Zineb BENDJILALI[a,b], Hafida BERRIAH[a,b], Houria LAKHDARI[a], Djahida LERARI[a] , Khaldoun BACHARI[a], Djillali MEZAOUI[c], Nour El Houda BENSIRADJ[d], Jean-Paul GUEGAN[e], Didier HAUCHARD[e,f]

[a]*Centre de Recherche Scientifique et Technique en Analyses Physico-chimiques (CRAPC), BP384, Bou-Ismail, RP 42004, Tipaza, Algeria.*

[b]*Faculté de Chimie, Université USTHB, 16111 Alger, Algerie*

[c]*Laboratoire Sciences des Matériaux, Faculté de Chimie, Université USTHB, 16111 Alger, Algerie*

[d]*Laboratoire de Chimie Théorique Computationnelle et Photonique, Faculté de Chimie, Université USTHB, 16111 Alger, Algerie*

[e]*Institut des Sciences Chimiques de Rennes, UMR CNRS 6226, Ecole Nationale Supérieure de Chimie de Rennes, 11 Allée de Beaulieu, 35708 Rennes, France*

[f]*Université Bretagne Loire, 1 Place Paul Ricoeur, 35000 Rennes, France*

[*]*Corresponding author: achour_t@yahoo.fr ; Tel.: +213.778.815.933, fax: +213.24.325.774*

Abstract

A novel bis-[1-(2-[(2-hydroxynaphthalen-1-yl) methylidene]amino}ethyl)-1-ethyl-3-phenylthiourea] Schiff base (L) and its binuclear palladium and ruthenium complexes have been prepared and characterized by ESI-MS, elemental analysis, NMR (^{1}H-NMR, ^{13}C-NMR, COSY, NEOSY and HSQC), FT-IR, ATR, UV-Visible spectra, TGA measurements, conductivity and cyclic voltammetry. The experimental results and the molecular parameters

calculated using DFT method revealed a square planar geometry around Pd and octahedral geometry around ruthenium metal.

The antibacterial activity of the ligand L and its complexes was evaluated against different human bacteria. In addition, the formation constants of the synthesized Schiff base-metal complexes and the systems formed with these chelates and cholesterol were estimated using spectrophotometric technique. The detection of cholesterol using novel Pd and Ru Schiff base complexes was studied using fluorometric method, and the measurements showed that the sensitive fluorometric response towards cholesterol analysis was determined using palladium complex. The limit of detection (LOD) of cholesterol calculated using this complex (4.6 µM) is lower (better) than LOD found using ruthenium complex (19.1 µM) and different compounds previously published around linear range of 0-5 mM.

Keywords: Schiff base, complexes of platinum group metals, stability constants, biological activities, fluorometric cholesterol sensor.

1. Introduction

The polydentate ligands such as Schiff bases lead to the formation of more stable complexes with metals of platinum group (Pd, Ru,…) in usual solvent [1, 2]. The use of these chelates is very important for application in medicinal field. Previously, the calix[4]arene–cholesterol derivatives with Schiff-base bridges were studied to investigate the behavior of these compounds towards cholesterol [3].

In recent years, significant progress has been realized on the impact of cholesterol on human health [4, 5]. Cholesterol concentration in human blood is clinically important in providing information for disease control and prevention [6]. Several studies have been conducted on the pathological states caused by imbalance of cholesterol [7-10]. Hence, the development of new

highly selective analytical methods is necessary for the determination of this biomolecule. Indeed, different methods were used to detect and determine cholesterol such as MS spectroscopic [11, 12], chromatographic [13, 14], electrochemical [15-18], spectrophotometric [7, 19] and fluorometric methods [20-23].

Recently, several works have been performed on the impact of inorganic complexes on diseases caused by increasing of concentration of cholesterol [24]. In addition, different materials have been used to detect this biomolecule, such as enzymatic silver/gold nanoparticles [25], enzyme/gold nanoparticules [26], silver nanoparticles [27], graphene quantum dots [28] and metal oxides-graphene [29, 30], bromine species [31], metallic oxides nanostructures [15, 32, 33], cyclodextrin-carbon nanotube composites [34], multi-wall carbon nanotubes [35] and metallic nanoparticles/carbon derivatives [36, 37].

To best of our knowledge, the detection of free cholesterol using metal complexes of platinum group metals like of palladim and ruthenium has not been reported till date. In the present work, after synthesis and characterization of novel bis-[1-(2-[(2-hydroxynaphthalen-1-yl)methylidene]amino}ethyl)-1-ethyl-3-phenylthiourea] ligand and its Pd and Ru complexes using different techniques such as ESI-MS, elemental analysis, FT-IR, UV–Visible, NMR, TGA and molecular modeling, we demonstrate that the fluorometric technique can be employed as an effective method to detect cholesterol using the synthesized ruthenium and palladium complexes. In addition, spectrophotometric technique was used to measure the stability constants of the synthesized Schiff base-palladium and Schiff base-ruthenium complexes, and also the systems formed with these chelates and cholesterol.

The main objective of the present work was to compare the efficiency of Ru and Pd-Schiff base complexes towards cholesterol detection with the previously developed systems.

2. Materials and methods

2. 1. Apparatus and reagents

Elemental analyses CHNS/O were recorded on a Perkin-Elmer Analyser 2400. The chloride and metal ions were analyzed using classical titration in the presence of $AgNO_3$ in addition to Atomic Absorption Spectroscopy (Agilent 240FS/240ZAA). The presence of these elements in the complexes has been confirmed by scanning electronic microscope coupled to EDS method (Hitachi TM-1000)). FT-IR and ATR spectra were recorded on a BRUKER α ALPHA-T spectrometer, in the spectral range 4000-400 cm^{-1}. All ^{1}H-NMR, ^{13}C-NMR and 2D-NMR measurements were performed at 25°C using a Bruker Avance III spectrometer operating at 400.13 MHz for ^{1}H, equipped with a BBFO probe with a Z-gradient coil and a GREAT 1/10 gradient unit. The ZG30 Bruker pulse program was used for ^{1}H-NMR, with a TD of 64 k, a relaxation delay d1 = 2 s. The spectrum width was set to 18 ppm. Fourier transform of the acquired FID was performed with apodization (lb<1 Hz). 2D-COSY experiments were acquired using the cosygpdqf pulse programs of the Bruker Library. Matrices consisting of 256–400 (t1)×2048 (t2) complex data points were recorded with a 1.5 s recovery delay (d1) and an AQ time of 0.25 s. Processing was performed with a QSINE function in both dimensions (SSB=0). 2D-HSQC (^{1}H-^{13}C) experiments were acquired using the hsqcetgpsisp.2 Bruker pulse program for high sensitivity with an AQ = 0.25 s, d1 = 1.5 s to 180 depending on the concentration. 256 experiences were acquired (t1). Fourier transform was performed in both dimensions with a QSINE function (SSB=2). ^{13}C-NMR spectra were recorded at 100.61 MHz where zgpg30 pulse program was used with 3k scans. TD was set to 32 k and a relaxation delay of 2 s for a spectral width of 235 ppm was used. Fourier transform was performed after apodization with an exponential function using a LB of 1 Hz.

2D NOESY experiments were acquired using the neosyph pulse program. The mixing time was of 1.5 s. Matrices consisting of 256 (t1)x2048 (t2) complex data points were recorded; 40

scans or more depending on the concentration were carried out per t1 increment with a 1.5 s recovery delay (d1) and an AQ time of 0.26 s. Processing was performed with a QSINE function in both dimensions (SSB=2).

The electronic spectra of ligand and coordination compounds were recorded on a SPECORD PLUS spectrophotometer in the range 200–1000 nm. The fluorescence spectra were obtained using VARIAN Model CARY Eclipse fluorescence spectrophotometer.

The mass spectrometry (positive ion electrospray ionization mass spectra) was performed using LC-MS/MS mass spectra in the presence of Q Exactive Hybrid Quadrupole-Orbitrap mass spectrometer.

The molar conductivity in DMSO (10^{-3} mol/L) was measured using a JENWAY- 4520 conductometer.

The thermogravimetric measurements (TGA) were recorded on SDT Q600 V20.9 Build 20 thermal analyzer under nitrogen atmosphere with a heating rate of 10 °C min^{-1} in 0-500 °C temperature range.

All reagents and solvents used in this work were of the highest purity and analytical grade from Sigma–Aldrich, Merck or Fluka chemical Companies. The different solutions were prepared in free CO_2 deionised water (resistivity ≥ 14 MΩ cm).

2. 2. Synthesis of ligand

The ligand (bis-[1-(2-[(2-hydroxynaphthalen-1-yl)methylidene]amino}ethyl)-1-ethyl-3-phenylthiourea]) was synthesized using the following protocol: in the first step, the intermediate was obtained by condensation reaction of 2-hydroxy-1-naphthaldehyde (20 mmol; 3.53 g) and triethylenetetramine (10 mmol; 1.5 mL) in absolute ethanol. The mixture was stirred at room temperature for 24 hours under inert atmosphere. The yellow precipitate (intermediate) was easily separated by filtration using methanol then dried in a

vacuum oven at 50 °C. In the second step, the dried yellow material (0.454 g) was dissolved in dichloromethane (20 mL) and was slowly added to a solution containing phenylisothiocyanate (2 mmol) in dichloromethane (10 mL). The reaction mixture was stirred and heated at 50 °C for 24 hours. The resulting product was cooled to room temperature, and the precipitate was filtered and washed with CH_2Cl_2 to obtain the desired ligand (L) as a yellow powder. The ligand was very soluble in DMF, DMSO, DCM, ethanol and acetone. However, it was slightly soluble in MeCN and insoluble in H_2O.

Yield: 0.55g (76%). m.p.:177.8 ºC. **ESI-MS** (in CH_3OH/CH_2Cl_2 (90%/10%)): m/z found (calc.): 725.2725 (725.2726) $[M+H]^+$ ($C_{42}H_{41}N_6O_2S_2$) (M refers to the molecular weight of L). **^{1}H-NMR (400 MHz, DMSO-d_6, 25 ˚C, ppm, δ):** 3.96 (s, broad, 4H, H_{14}), 4.08 (s, broad, 4H, H_{17}), 4.13 (s, broad, 4H, H_{15}), 6.72 (d, 2H, J=9.4 Hz, H_3), 7.13 (m, 2H, H_{23}), 7.18 (ddd, 2H, J=8.0 Hz, H_{10}), 7.22–7.26 (m, 8H, H_{21}, H_{22}, H_{24}, H_{25}), 7.39 (ddd, 2H, J=8.5 Hz, H_9), 7.62 (dd, 2H, J=8.0 Hz, H_{11}), 7.72 (d, 2H, J=9.4 Hz, H_4), 8.05 (d, 2H, J=8.5 Hz, H_8), 9.10 (d, 2H, J=10 Hz, H_{12}), 9.50 (s, broad, 2H, H_{19}), 13.88 (s, broad, 2H, terminal phenolic OH: H_1). **NOESY** shows correlation between (H_{12}) and (H_8). **^{13}C-NMR (100 MHz, DMSO-d_6, 25 ˚C, ppm, δ):** 40.38 (C_{17}); 48.51 (C_{15}); 48.56 (C_{14}); 106.10 (C_7); 118.61 (C_8); 122.33 (C_{10}); 125.26 (C_3);125.31 (C_5); 125.33 (C_{21}); 126.88 (C_{23}); 127.91 (C_9); 127.95 ($C_{22,\ 24,\ 25}$); 128.90 (C_{11}), 134.45 (C_6); 137.23 (C_4); 140.30 (C_{20}); 159.60 (C_{12}); 177.65 (C_2);181.29 (C_{18}). **COSY-NMR (100 MHz, DMSO-d_6, 25 ˚C, ppm, δ):** 9.5 (NH); 13.88 (OH). **^{1}H-^{13}C HSQC-NMR (100 MHz, DMSO-d_6, 25 ˚C, ppm, δ):** 3.96:8.56 (H_{14}:C_{14}); 6.72:125.26 (H_3:C_3); 7.13 :126.88 (H_{23}:C_{23}); 7.18:122.33 (H_{10}:C_{10}); 7.22-7.26:127.95 ($H_{21,\ 22,\ 24,\ 25}$:$C_{21,\ 22,\ 24,\ 25}$); 7.39:127.91 (H_9:C_9); 7.62:128.90 (H_{11}:C_{11}); 7.72:137.23 (H_4:C_4); 8.05:118.61 (H_8:C_8). **UV-Vis (DMSO, λ :nm (ε :L/mol cm)):** 272 (48439); 306 (31676); 404 (23294); 424 (24104). **Fluorescence (DMSO, λ_{ex} (λ_{em}):nm):** 300 (352). **FT-IR:cm^{-1} (ATR: cm^{-1}):** 3430 (-) υ(O-H) $H_2O_{Hydration}$;

3241 (3223) υ(O-$H_{phenolic}$); 3058 (3055) υ(N-H); 2820-2960 (2810-2985) υ(C-H); 1620 (1624) υ(C=N); 1192 (1183) υ(C-O); 1074 (1074) υ(C-N); 838 (838) δ(C=S).

2. 3. Synthesis of palladium and ruthenium complexes

The palladium complex was prepared by mixing ligand (L) (1 mmol) in 10 mL of heated ethanol in the presence of K_2PdCl_4 (2 mmol), which was prepared by mixing 0.177 g of $PdCl_2$ with 0.149 g of KCl in 50 mL of distillated water. The mixture was refluxed for 6 hours. The formed precipitate was filtered, washed with distilled water and dried under vacuum oven.

Yield: 0.69g (69%). m.p.: 290 ºC. **Λ ($Ω^{-1}$. cm^{-1}. mol^{-1})**: 0.06. Anal. Calc. (%). $[Pd_2LCl_2].2H_2O$ (Pd complex: $C_{42}H_{38}N_6O_2S_2Cl_2Pd_2,2H_2O$) (Mw = 1042.69 g/mol): C:48.38; H:4.06; N:8.06; S:6.15; O:6.14; Cl: 6.80; Pd: 20.41. Found (%): C:48.13; H:4.28; N:8.26; S:5.83; O:6.52; Cl:6.38; Pd: 20.60. **^{1}H-NMR (400 MHz, DMSO-d_6, 25 ˚C, ppm, δ):** 2.53 (s, broad, 4H, H_{14}), 3.18 (s, broad, 4H, H_{17}), 3.89 (s, broad, 4H, H_{15}), 7.02 (s, 2H, H_3), 7.15 (s, 2H, H_{23}), 7.24–7.27 (m, 8H, $H_{21, 22, 24, 25}$), 7.44 (ddd, 2H,J=8.0 Hz, H_9), 7.61 (ddd, 2H,J=8.0 Hz, H_{10}), 7.87 (dd, 2H,J=8.0 Hz, H_8), 8.12 (dd, 2H, J=8.9 Hz, H_{11}), 8.93 (d, 2H, J=8.3 Hz, H_{12}), 10.80 (s, broad, 2H, H_{19}), 11.99 (small integration value: 0.12, due to trace impurities present in the solvent). **^{13}C-NMR (100 MHz, DMSO-d_6, 25 ˚C, ppm, δ):** 40.36 (C_{17}); 110.65 (C_7); 118.92-133.88 ($C_{3, 5,8, 9, 10, 11}$ and $C_{21, 22, 23, 24, 25}$); 138.62 (C_6); 144.44 (C_4); 145.40 (C_{20}); 158.30 (C_{12}); 169.25 (C_2); 201.70 (C_{18}); the peaks of C_{15} and C_{17} are conflated with those from DMSO; **UV-Vis (DMSO, λ :nm (ε :L mol^{-1} cm^{-1})):** 301 (10191); 415 (1614). **FT-IR:cm^{-1} (ATR: cm^{-1}):** 3300-3600 (3300-3600) υ(O-H)$_{H2O}$; 3125 (3103) υ(N-H); 1630 (1630) υ(C=N); 1250 (1210) υ(C-O); 862 (881) δ(C=S).

Aqueous solution of $RuCl_3.H_2O$ (0.5 mmol; 5 mL of hot distilled water) was added drop wise to a hot solution containing our synthesized ligand (0.25 mmol; 10 mL of ethanol) with a

molar ratio of 2:1 metal:ligand. The reaction mixture was stirred and refluxed at 70-75 °C for 4 hours until a color change was observed. The formed precipitate was filtered, washed with distilled water and dried under vacuum oven at 50 °C.

Yield: 0.18g (65%). m.p.: 227 ºC. **Λ (Ω^{-1}. cm^{-1}. mol^{-1})**: 14.38. Anal. Calc. (%). $[Ru_2LCl_4(H_2O)_2].4H_2O$ (Ru complex: $C_{42}H_{42}N_6O_4S_2Cl_4Ru_2,4H_2O$) (Mw = 1174.96 g/mol): C:42.93; H: 4.29; N:7.15; S:5.46; O: 10.89; Cl: 12.07; Ru:17.21. Found (%): C:42.23; H:3.86; N:7.66; O: 10.95; S:5.73; Cl: 12.34; Ru:17.23.

^{1}H-NMR (400 MHz, DMSO-d_6, 25 ˚C, ppm, δ): 2.53 (s, broad, 4H, H_{14}), 3.39 (s, broad, 4H, H_{17}), 3.81 (s, broad, 4H, H_{15}), 7.23 (s, 2H, H_3), 7.25 (s, 2H, H_{23}), 7.27–7.33 (m, 8H, $H_{21, 22, 24, 25}$), 7.42 (ddd, 2H, J=8.0 Hz, H_9), 7.47 (ddd, 2H, J=8.0 Hz, H_{10}), 7.61 (dd, 2H,J=7.5 Hz, H_8), 7.87 (dd, 2H, J=8.0 Hz, H_{11}), 8.12 (d, 2H, J=9.0 Hz, H_4), 8.92 (d, 2H, J=8.5 Hz, H_{12}), 10.83 (s, broad, 2H, H_{19}), 11.99 (small integration value: 0.16, due to trace impurities present in the solvent). **^{13}C-NMR (100 MHz, DMSO-d_6, 25 ˚C, ppm, δ):** 40.72 (C_{14}); 103.70 (C_7); 119.04 (C_{23}); 119.06 (C_3); 122.56 (C_{12}); 124.20 (C_5); 124.64 (C_9); 127.18-127.70 ($C_{21, 22, 24, 25}$); 129.26 (C_{11}); 129.52 (C_8); 130.00 (C_{10}); 134.51 (C_6); 138.76 (C_4); 151.36 (C_{20}); 168.25 (C_2); 193.12 (C_{18}); the peaks attributed to C_{15} and C_{17} are conflated with those of DMSO. **^{1}H-^{13}C HSQC-NMR (100 MHz, DMSO-d_6, 25 ˚C, ppm, δ):** 2.53:40.72 (H_{14}:C_{14}); 7.23:129.52 (H_3:C_3); 7.25:119.04 (H_{23}:C_{23}); 7.47:130.00 (H_{10}:C_{10}); 7.27–7.33:127.18-127.70 ($H_{21, 22, 24, 25}$:$C_{21, 22, 24, 25}$); 7.42:124.64 (H_9:C_9); 7.87:129.26 (H_{11}:C_{11}); 8.12:138.76 (H_4:C_4); 7.61:129.52 (H_8:C_8); 8.92:122.56 (H_{12}:C_{12}). **UV-Vis (DMSO, λ :nm (ε :L/mol cm)):** 313 (9631); 402 (1717); 427 (1367); 687 (82). **FT-IR:cm^{-1} (ATR: cm^{-1}):** 3300-3600 (3300-3600) υ(O-H_{H2O}); 3153 (3103) υ(N-H); 1630 (1632) υ(C=N); 1248 (1200) υ(C-O); 828 (827) δ(C=S).

2. 4. Antioxidant activity

The antioxidant activity of the products has been evaluated using DPPH method.

IC_{50} values were graphically determined by linear regression (IC_{50}: the concentration required that inhibits the reaction up to 50% of the uninhibited maximum value).

A stock solution containing DPPH in methanol (40 mg/L) was prepared and kept in the dark at 6 ° C. Set solutions containing 1mg/mL of our synthesized compounds have been prepared in DMSO and were diluted to obtain concentrations ranging from 500 µg/mL to 1µg/mL. Then, 1 mL of DPPH solution was added to 3 mL of each sample. After stirring, the products were placed in the dark at room temperature for 30 minutes. Finally, the absorbance was measured at 517 nm using UV-Visible technique.

The scavenging activity of samples was calculated using the following equation:

$$\text{Scavenging activity } (\%) = \left(\frac{A_0 - A}{A_0}\right) \times 100$$

where A_0 is the absorbance of the control solution, and A is the absorbance in the presence of sample solution.

2. 5. Antibacterial activities

Antibacterial activities of the ligand and its complexes was investigated against five bacterial strains (*Methicillin-Resistant Staphylococcus Aureus*: *MRSA* (ATCC 43300 (Gram +)), *Methicillin-Sensitive Staphylococcus Aureus*: *MSSA* (ATCC 25923 (Gram +)), *Pseudomonas Aeruginosa: P. Aeruginosa* (ATCC 27853 (Gram -), *Micrococcus sp: µ.coccus* (Gram +) *and Escherichia coli: E. coli* ATCC 25922 (Gram -)) using the disk diffusion method [38]. Sterile filter paper discs (9 mm diameter) were impregnated with 25 µL of test sample (10 mg/mL in DMSO), and were placed on the previously marked zones in the agar plates pre-inoculated with test bacteria. Then, the disc was introduced on the layer of the seeded agar plate. For each bacterial strain, negative controls were maintained, and a negative effect was observed with DMSO. The bacterial plates were incubated at 37°C for 24 hours.

The antibacterial activity was evaluated by measuring the diameter of inhibition zones**.**

2. 6. Spectrophotometric titrations

For each complex, a stock solution was prepared using buffer disodium hydrogen phosphate/sodium dihydrogen phosphate (Na_2HPO_4/NaH_2PO_4: 0.1 M) in water-ethanol (25/75% vol./vol.) solution.

The titration experiments were carried out in the following way:

For the system of ligand-metal, 2.31 mL of the ligand was pipetted into a quartz cuvette and volumes of 5 µL of metal (0.01 M) were added to each sample using a micro-syringe.

For the system of complex-cholesterol, different volumes of cholesterol (0.01 M) were added to 2.3 mL of each complex using an automatic pipette.

2.6.1. Stability constants of the complexes

The stability of the complexes was performed considering metal-ligand stoichiometry equal 2: 1:

$$L + 2M \leftrightarrow LM_2 \text{ with } K = \frac{[LM_2]}{[M]^2[L]} \text{ .....(1)}$$

In the absence of the metal, the absorbance (A_0) is given by Beer Lambert equation:

$$A_0 = \varepsilon_L \ell [L]_0 \text{ .....(2)}$$

with $[L]_0$ is the concentration of ligand in the absence of metal cations.

After addition of metal ions, the absorbance A can be written:

$$A = \varepsilon_L \ell [L] + \varepsilon_{LM_2} \ell [LM_2] \text{ .....(3)}$$

Reporting $[L] = [L]_0 - [LM_2]$, equation (3) may be given by the following equations:

$$A = \varepsilon_L \ell [L]_0 + \varepsilon_{LM_2} \ell [LM_2] - \varepsilon_L \ell [LM_2] \text{ .....(4)}$$

$$A = \varepsilon_L \ell [L]_0 + (\varepsilon_{LM_2} - \varepsilon_L) \ell [LM_2] \text{ .....(5)}$$

The rearrangement of equations (4) and (5) leads to the following form:

$$A - A_0 = (\varepsilon_{LM_2} - \varepsilon_L)\ell[LM_2] \text{.....(6)}$$

Reporting $[LM_2] = K[M]^2[L]$, equation (6) becomes:

$$A - A_0 = (\varepsilon_{LM_2} - \varepsilon_L)\ell K[M]^2[L] \text{.....(7)}$$

From equations (8) and (9):

$$K[M]^2[L] = [L]_0 - [L] \text{.....(8)}$$

$$[L] = \frac{[L]_0}{1 + K[M]^2} \text{.....(9)}$$

Equation (7) becomes:

$$A - A_0 = (\varepsilon_{LM_2} - \varepsilon_L)\ell K[M]^2 \left(\frac{[L]_0}{1 + K\left([M]^2\right)}\right) \text{.....(10)}$$

The inverse of equation (10) yields the Benesi-Hildebrand equation:

$$\frac{1}{A - A_0} = \frac{1 + K[M]^2}{(\varepsilon_{LM_2} - \varepsilon_L)K\ell[M]^2[L]_0} \text{.....(11)}$$

with $\ell = 1cm$, equation (12) was obtained:

$$\frac{1}{A - A_0} = \frac{1}{(\varepsilon_{LM_2} - \varepsilon_L)K[M]^2[L]_0} + \frac{1}{(\varepsilon_{LM_2} - \varepsilon_L)[L]_0} \text{.....(12)}$$

From the absorbance curves, $\frac{1}{A - A_0}$ versus $\frac{1}{[M]^2}$ was plotted, and the stability constants of the complexes were determined.

2. 6. 2. Interaction of the complexes with cholesterol

In this part, UV-Visible method was used to evaluate the interaction complexes-cholesterol. The variation in the absorbance observed in electron spectra was used to determine the stoichiometry of complex-cholesterol systems and their formation constants. In the solution,

the complex-cholesterol compound was formed between the LM_2 complex and cholesterol (*chol*) by the following chemical equilibrium:

$$LM_2 + chol \leftrightarrow LM_2 - chol$$

The formation constant is given by the equation:

$$K = \frac{[LM_2 - chol]}{[LM_2][chol]}$$

Considering the stoichiometry of complex:cholesterol equal 1:1 and proceeding through the same previous steps (section 2.6.1.), the Benesi-Hildebrand equation was obtained and the formation constant can be calculated:

$$\frac{1}{A - A_0} = \frac{1}{K\Delta\varepsilon[LM_2][chol]} + \frac{1}{\Delta\varepsilon[LM_2]_0}$$

2. 7. Fluorometric titrations

The fluorescence technique was used to calculate the quenching constants and limit of detection of cholesterol (*LOD*).

The intensity of fluorescence was determined between 300 and 750 nm with 5/5 excitation/emission slits. The fluorescence spectrum was recorded for each concentration of cholesterol added to the complex solution (equilibrium time: 10 min).

The fluorescence quenching phenomenon is defined by the Stern-Volmer equation

$$\frac{I_0}{I} = 1 + K_{SV}[Q]$$

where I_0 and I are the fluorescence intensity values of free complex and the intermediate values during the titration, respectively.

K_{SV}: quenching constant (Stern-Volmer constant);

[Q]: concentration of the quencher (cholesterol).

3. Results and discussion

3.1. Charaterization of the ligand and its complexes

3. 1. 1. Infrared spectrometry

The FT-IR (Fig. 1) and ATR (Fig. 1S) spectra of the ligand (L) (Scheme 1) showed a broad band at 3416 cm^{-1}, due to the stretching vibrations of OH of phenolic groups. The peak appeared at 3241 cm^{-1} is assigned to the stretching vibrations of NH groups. The intense bands observed around 1620 cm^{-1} are attributed to the stretching vibration of the C=N functions. The peaks observed at 1535 and 1357 cm^{-1} are assigned to the deformation vibrations of NH and OH groups (δ NH and δ OH), respectively. The stretching vibration of C=C bonds in the aromatic ring was observed at 1446 cm^{-1}. The presence of C=S groups in the ligand structure was confirmed by the bands at 838 and 1463 cm^{-1}. The bands between 1200 and 1070 cm^{-1} are assigned to the vibration of C-N and C-O bonds.

The infrared data (FT-IR and ATR) of the ligand are summarized in table 1S.

To identify the coordination sites involved in chelating process, infrared spectra of the metal complexes were compared with that of the ligand (Fig. 1, 1S and Table 1S).

FTIR and ATR spectra of all complexes showed broad bands in the range 3430-3360 cm^{-1}, which may be assigned to OH of coordination and hydration water molecules associated with complexes [39].

The band at 3416 cm^{-1} in the free ligand spectrum, assigned to the phenolic OH groups, was disappeared in the complexes, suggesting the coordination of metal ion with deprotonated phenolic group of ligand.

The stretching vibration υ_{N-H} appeared at 3241cm^{-1} in the spectrum of free ligand is shifted in the spectra of the complexes (3120-3160 cm^{-1}), meaning that the vibration of NH group is influenced by binding of metal to C=S group.

The stretching vibrations of C=N ($\upsilon_{C=N}$: 1620 cm^{-1}) was shifted to a higher wavenumber (1630 cm^{-1}) after complexation, indicating that the metal is bonded with the nitrogen of the azomethine group [40].

The stretching vibration of C-O band in the ligand is shifted to higher frequencies (around 60 cm^{-1}) in the complexes, suggesting the coordination of oxygen of phenolic group to the metal ion.

The band at 838 cm^{-1} assigned to $\upsilon_{C=S}$ in the ligand spectrum is shifted to 828 cm^{-1} and 862 cm^{-1} in the Ru and Pd complexes spectra, respectively, indicating the involvement of sulfur atoms in the coordination of ligand with metal [41].

The involvement of sulfur, oxygen and nitrogen atoms in coordination of L with metal ions is confirmed by the appearance of new bands (low intensity) in the ranges 503-510 cm^{-1}, 522-543 cm^{-1} and 414-430 cm^{-1} due to $\upsilon_{M-S,}$ υ_{M-N} and υ_{M-O}, respectively [42].

All these results indicated that Ru and Pd metals are bonded through nitrogen of C=N, sulfur of C=S and oxygen of phenolic group of L.

3. 1. 2. NMR spectrometry

The proton, carbon and two dimentional magnetic resonance spectra of Schıff base ligand L were reported in Fig. 2 and 2S, . The signals of protons for free ligand showed tow important peaks appeared at 9.50 ppm and 9.10, which have been attributed to -NH-C=S [43] and -CH=N groups, respectively. The proton signals observed at 13.88 ppm (s, broad, 2H), 4.13 ppm (s, broad, 4H) and 3.96 ppm (s, broad, 4H) are assigned to –OH, -CH_2-N- and C=N-CH_2-

groups, respectively. The presence of C=N, C-OH and C=S groups was confirmed with carbon signals observed at 159.60 ppm, 177.65 ppm and 181.29 ppm, respectively.

The comparative study between the NMR spectra of the free ligand and its metal complexes (Fig. 2 and 2S) showed the disappearance of the signal at 13.88 ppm assigned to the phenolic proton of free ligand in the spectra of the complexes, confirming the involvement of phenolic groups in its deprotonated form in the coordination process with metal ions.

The signal of the NH groups (9.50 ppm) near C=S function is shifted in the spectra of the complexes (around 10.80 ppm) (Fig. 2b,c), indicating the coordination of the ligand to the metals through the sulfur atom.

The signal due to the azomethine proton (CH=N) (9.10 ppm in the free ligand) is shifted to 8.93 and 8.92 ppm in the spectra of Pd and Ru complexes, respectively. This observation supported the involvement of the nitrogen atom of azomethine group in the formation of the complexes.

The desapparence of the signal at 4.5 ppm in the spectrum of plladium complex reveals the absence of the coordinted water molecules in the structure of Pd complex.

The analysis of the NMR results showed that the signal of ligand observed at 159.60 ppm (C=N carbon) (Fig. 2a) was shifted in the complexes spectra, confirming the coordination of L to metal with azomethine groups. The signal at 181.29 ppm due to the thione carbon band (C=S) was shifted to 193.12 ppm in the spectrum of Ru complex (Fig 2Se), and to 201.70 ppm in the spectrum of Pd complex (Fig 2Sf), indicating the coordination of the ligand to the metals through sulfur atom.

^{1}H-^{13}C HMBC-NMR spectrum of Ru complex showed a good correlation between the protons and the associated carbons. This technique confirms that the signal attributed to the carbon of C=S band coupled to the proton of N-H witch observed around 10.8 ppm. This result indicates that the ligand is complexed with metal ion through sulfur atom of thione group.

3. 1. 3. UV-Visible spectrophotometry

The absorption spectra of the ligand and its complexes were recorded in DMSO in the wavelength range of 250–1000 nm.

The electronic spectrum of the ligand (Fig. 3) showed four absorption bands, the first shoulder band at 272 nm (ε= 48439 $L.mol^{-1}. cm^{-1}$) and the second at 306 nm (ε= 31676 $L.mol^{-1}. cm^{-1}$) were ascribed to π→π∗ transitions, while the third and the fourth observed at 404 nm (ε= 23294 $L.mol^{-1}. cm^{-1}$) and 424 nm (ε= 24104 $L.mol^{-1}. cm^{-1}$) are attributed to n→π∗ transitions, respectively.

Electronic spectrum of binuclear Ru complex (Fig. 3) showed an intense absorption at 313 nm (ε= 9631 $L.mol^{-1}. cm^{-1}$) due to n→π∗ transition of azomethine group. In the visible region, the bands observed at 402 nm (ε= 1717 $L.mol^{-1}. cm^{-1}$), 427 nm (ε= 1367 $L.mol^{-1}. cm^{-1}$) and 687 nm (ε= 82 $L.mol^{-1}. cm^{-1}$) are attributed to LMCT, $^{2}T_{2g}\rightarrow{}^{4}T_{1g}$ and $^{2}T_{2g}\rightarrow{}^{4}T_{2g}$, $^{2}A_{1g}$ d-d transition, respectively. The electronic absorption results of Ru complex (Table 2S) indicating octahedral environment around ruthenium [44, 45].

The electronic spectrum of Pd complex exhibit diamagnetic character confirming the square planar geometry with L. The absorbance at 415 nm (24096 cm^{-1}, ε= 1614 $L.mol^{-1}. cm^{-1}$) corresponds to $^{1}A_{1g} \rightarrow {}^{1}A_{2g}$ d-d transition. The nature of this band suggests square planar geometry around Pd [46].

The absorbance observed at 301 nm (33222 cm^{-1}, ε= 10191 $L.mol^{-1}. cm^{-1}$) due to the intra ligand π→π∗ transition in the complex. The shift of this band compared to that observed on the spectrum of the ligand confirms the coordination of Pd with CH=N and C=S groups [47].

3. 1. 4. Fluorescence spectrometry

The emission spectra of the ligand and its complexes were investigated at room temperature (298 K) in ethanol solution (Fig. 4).

Fluorescence emission spectrum of the ligand showed a broad emission band around 355 nm from the excited state charge transfer intra molecular, assigned to the $\pi \rightarrow \pi*$ intra ligand fluorescence. The position of the emission band of the ligand is dependent both the nature of the donor moiety and the length of the conjugated chain.

The highest fluorescence intensity of L confirms the fluorescent yellow color of this Schiff base.

The fluorescence emission spectra of palladium and ruthenium complexes reported in Fig. 4 showed that the emission bands were located at 400 nm and 358 nm, respectively, due to intraligand fluorescence $\pi \rightarrow \pi^*$.

The fluorescence intensity of free ligand is characterized by the occurrence of a photo-induced electron transfer (PET) process due to the presence of the lone pair of the donor atoms. PET process is prevented by the complexation of the ligand with metal ions. Thus, the fluorescence intensity can be increased or decreased upon coordination. The ligand binding to the palladium ion increases the conformational rigidity of the ligand (formation of stable Pd complex) [48] and decreases the intensity of fluorescence with non-radiative energy loss.

The palladium complex exhibits the lowest fluorescence intensity, while the highest intensity was obtained for ruthenium complex (less stable complex), indicating that the ligand has different binding affinity for some transition metals by fluorometric method [49].

3. 1. 5. Physical properties, elemental analysis and molar conductance

The formed complexes are stable in air and at room temperature. They are soluble in ethanol and in most organic solvents such as DMSO and DMF. However, these complexes are insoluble in water, and slightly soluble in acetone and dichloromethane (DCM).

On the basis of elemental analysis (Anal. Found %), the complexes showed the composition reported below in section 2.3. The obtained results are in the good agreements with those calculated (Anal. Cal. %), confirming the proposed molecular formulae.

The conductivity of all complexes is determined in DMSO solution (10^{-3} M). The obtained values (Pd complex: 0.06 Ω^{-1}. cm^{-2}. $mol^{-1}$and Ru complex: 14.38 Ω^{-1}. cm^{-2}. mol^{-1}) showed that these compounds are non-electrolytes.

The chemical composition of the complexes (C, N, O, S, Cl, Pd and Ru) was confirmed by the appearance of their characteristic peaks on energy dispersive X-ray diffraction (EDS) diagrams (Fig. 3S).

3. 1. 6. Thermal analysis of the complexes

The thermal decomposition studies of Ru and Pd complexes were carried out in nitrogen atmosphere in the temperature range of 30-500 ºC. The TGA curves are given in figure 5. TGA curve of Ru complex showed weight loss 6.51 % (calc. 6.52 %) in the temperature range 28-78 °C, this is due to loss of four molecules of water of hydration. In second step, two coordinated water molecules are liberated in the temperature range 78-141 °C with weight loss of 3.20 % (calc. 3.21 %). The third decomposition step of the complex in the temperature range 141-184 °C shows a weight loss of 9.70 % (calc. 9.61 %), which correlates with the loss of four coordinated chloride molecules. The decomposition of the rest of the ligand with a weight loss of 63.32 % (calc. 63.52 %) was observed between 184 °C and 315 °C. For T> 325 °C, the decomposition of Ru oxide (Ru_2O_3) was noted with weight loss of 21.94 % (calc. 21.53 %), which confirms the binuclear complex.

The TGA curve of Pd complex (Fig. 5) showed that the first stage of degradation between 22 -110 °C with weight loss of 3.62 % (calc. 3.75 %) is due to loss of tow hydrate water molecules. In second step, two coordinated Chlorine atoms are liberated in the temperature

range 140-210 °C with weight loss of 7.31 % (calc. 7.05 %). The third degradation of the complex in the temperature range 222-320°C shows a weight loss of 44.80 % (calc. 44.30 %), which correlates with the decomposition of the organic part. The recorded residual masse suggests the presence of Pd_2O_2 oxide as final decomposition.

Based on all characterizations, the descriptive synthesis schemes of Schiff base ligand L and its complexes are reported below:

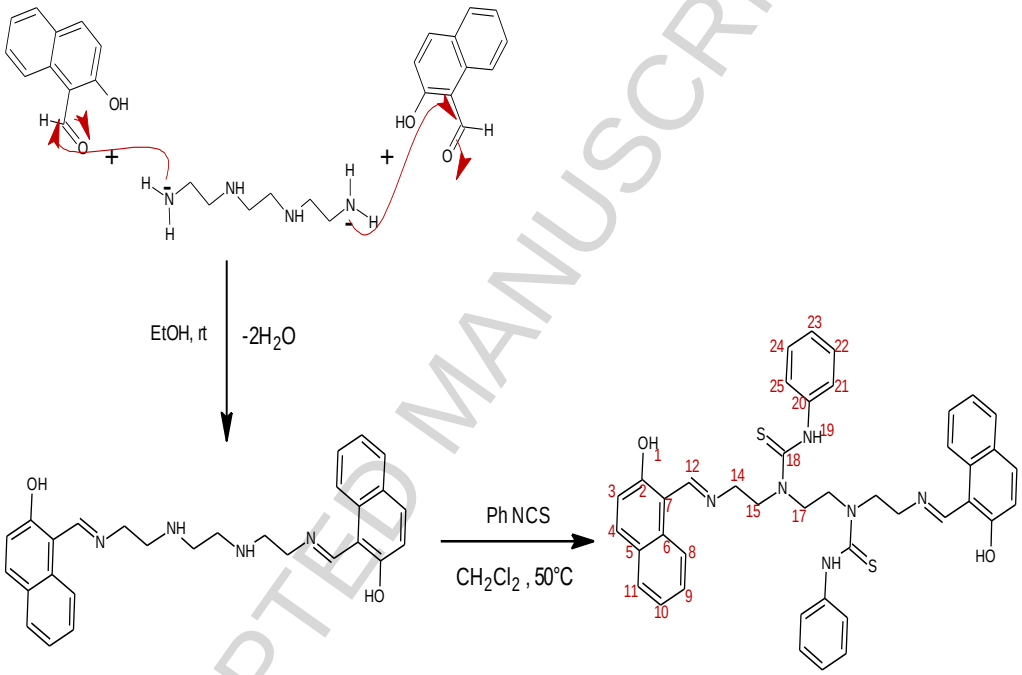

Scheme 1. Synthetic route of ligand (L).

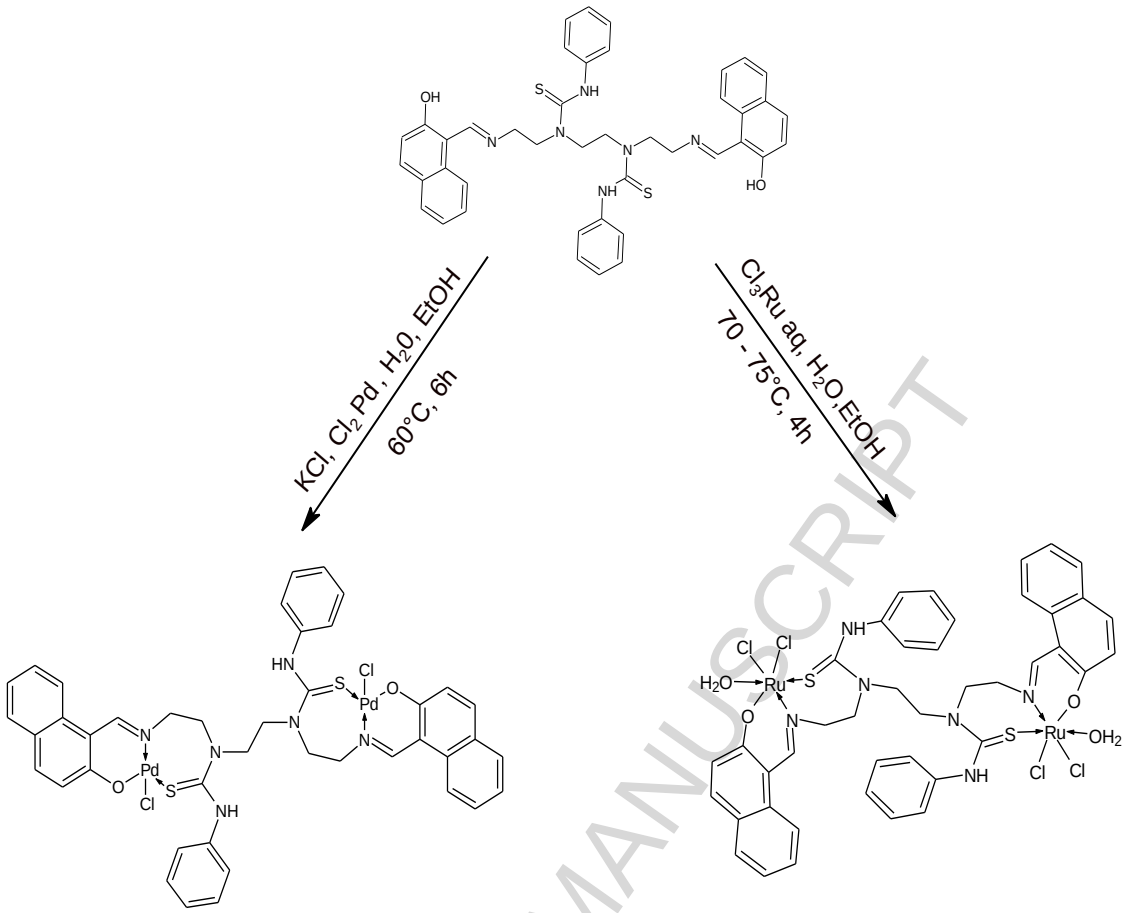

Scheme 2. Synthetic route of Pd and Ru complexes.

3. 3. Theoretical study (DFT)

3. 3. 1. Geometry optimization

The optimization geometries and vibrational frequency analysis were performed using DFT method with the M06 level [50] and relativistic effective core potential basis set of double zeta quality, Lanl2dz [51], as implemented in Gaussian 03 program package [52]. Each geometry optimization was completed by a calculation of harmonic vibrational frequencies to confirm the most stable geometry. The studied forms of Ru and Pd complexes were characterized as minima (no imaginary frequency) in their potential energy surface through harmonic frequency analysis.

The selected bond distances, valence and dihedral angles for the six mononuclear and binuclear optimized forms of Pd and Ru complexes (Mononuclear Pd complex: (Pd-NOSCl)$_1$:form1; (Pd-NNOS)$_1$: form2; (Pd-NNSCl)$_1$:form3, Binuclear Pd complex: (Pd-NOSCl)$_2$:form4; (Pd-NNOS)$_2$:form5, (Pd-NNSCl)$_2$:form6, Mononuclear Ru complex: (Ru-NSOO$_{(H2O)}$ClCl)$_1$:form1; (Ru-NNOSClCl)$_1$: form2; (Ru-NSOClClCl)$_1$:form3, Binuclear Ru complex: (Ru-NSOO(H_2O)ClCl)$_2$:form4; (Ru-NNOSClCl)$_2$:form5; (Ru-NSOClClCl)$_2$:form6) are reported in tables 3S and 4S.

The values of minimized energy of the different proposed geometries (mononuclear and binuclear forms) of Ru and Pd complexes (Table 1) show that the form4 of these chelates exhibits low energy and large gap (form4 of Pd ccomplex: ΔE= 1.36 eV, form4 of Ru complex: ΔE= 1.38 eV) compared to the other forms, indicating that the binuclear structure is more stable than mononuclear structure.

The optimized structures of the studied complexes are reported in the figures 6a and 6d.

3. 3. 2. HOMO and LUMO

Some parameters such as highest occupied molecular orbitals (HOMO) and lowest unoccupied molecular orbitals (LUMO) of the Ru and Pd complexes have been calculated (Table 1). Figures 6b,c,e,f show the frontier orbitals shape. The HOMO density of the stable form of the Pd (Fig. 6b) and Ru (Fig. 6e) complexes is distributed over the metallic element, oxygen, nitrogen and sulfur atoms, and especially around triethylenetetramine group. For the LUMO level (Fig. 6c, f), we observed that the electronic density is localized around a single part of metal complexes.

3. 4. Electrochemical study

The electrochemical behavior of the binuclear ruthenium and palladium complexes in DMSO were studied by cyclic voltammetry with a scan rate of 20 mV/s, using a platinum working electrode, glassy carbon counter electrode and saturated Ag/AgCl as a reference electrode.

The cyclic voltammogram of the Pd complex (Fig. 7) exhibits a cathodic wave (E_{pc}= -0.45V) combined with an anodic wave (E_{pa}= -0.66V) assigned to the reduction of Pd(II) to Pd(I). The oxidation and reduction processes observed at E_{pa} = -1.04 V and E_{pc} = -1.32 V are assigned to C=S groups of the ligand.

In addition to the redox waves of the ligand, the voltammogram of the Ru complex (Fig. 7) shows two redox couples. The first (E_{pa}=0.64 V; E_{pc}=0.50 V) is attributed to Ru (IV)/Ru (III) redox couple, and the second at E_{pa}=-0.24V and E_{pc}=-0.56 V is assigned to Ru (III)/Ru (II) redox couple.

The electrochemical behavior of the complexes versus scan rate (Fig. 4a,cS) shows that the peak current intensity increases steadily with increasing scan rate.

Plotting current versus square root of scan rate (Fig. 3b,dS), a linear regression equations were reported: $i_{pa} = 0.5916v^{0.5} - 1.6720$ $(R^2 = 0.991)$ for Ru complex and $i_{pa} = 0.649v^{0.5} + 2.763$ (R^2=0.988) for Pd complex. These results showed that the electrochemical process is controlled by the diffusion phenomenon.

3. 5. Antioxidant activity

The antioxidant activities of the investigated compounds and the standard Trolox [53] were evaluated on the basis of the radical scavenging effects of the stable DPPH (1,1-diphenyl-2-picryl hydrazyl) free radical. The radical scavenging effects of antioxidants on DPPH are due to their hydrogen or electron donation, which causes an absorbance at 517 nm. After reaction between the compounds (ligand and complexes) and DPPH radical, the antioxidants caused a

significant decrease in the absorbance of the DPPH radical, indicating higher free radical scavenging activity [54] (Fig. 8a).

All complexes showed an important antioxidant activity (the ligand does not exhibit antioxidant activity). The determined antioxidant activities showed that Ru complex has significant antioxidant activity (IC_{50}=3.46±0.02 µg/mL) compared to that of Pd complex (IC_{50}=13.68±0.05 µg/mL), indicating a higher scavenging activity towards hydroxyl radical. This may be explained by binding of DPPH with metal ions (neutralization of the single electron). The presence of the metal ions substantially gives the antioxidant activities of these complexes.

3. 6. Antibacterial activity

The comparison between the average activity values of ligand (L) and that of its corresponding metal complexes (Fig. 8b) revealed that the activity was increased upon coordination of L with metal ions. Ruthenium complex was more effective than L and palladium complex, it possessed a remarkable activity on the tested bacteria, especially against *Methicillin-Resistant Staphylococcus Aureus* (22 mm), *E. coli* (20 mm) and *Methicillin-Sensitive Staphylococcus Aureus* (18 mm). While, Pd complex exhibited activities on *Methicillin-Resistant Staphylococcus Aureus* (19 mm) and *Methicillin-Sensitive Staphylococcus Aureus* (16 mm).

3. 7. Stability of the complexes and interaction of complex-cholesterol

3. 7. 1. Stability study of Pd and Ru complexes

To evaluate the stability of the formed Ru and Pd complexes with ligand (L), the titration curves (absorbance (*A*) vs. wavelength (λ/nm)) and $\frac{1}{A-A_0}$ *vs.*$(\frac{1}{[M]^2})$ were plotted. Figures 9

and 5S showed that the absorbance substantially increases with increasing metal concentrations, indicating that the metal ion is bonded to ligand.

Calibration curves in figures 9b,c showed that $1/(A-A_0)$ was directly proportional to $1/[M]^2$ for Ru and Pd complexes, with a linear regression equation of $\frac{1}{A-A_0} = 2.562\times10^{-8}\frac{1}{[M]^2} + 0.757$ (R^2=0.981) and $\frac{1}{A-A_0} = 2.303\times10^{-8}\frac{1}{[M]^2} + 3.619$ (R^2=0.992), respectively.

The analysis of the obtained results shows that the complexes of palladium and ruthenium were formed at a 2:1 metal to ligand ratio, and Pd complex ($logK_s$=8.2) are more stable than the complex prepared with Ru ion ($logK_s$=7.4) (Table 2). This result confirms the stability thermal in the solid state (high temperature: melting temperature and TGA analysis) of the palladium complex.

3. 7. 2. Interaction of complex-cholesterol

The interaction of cholesterol with Ru and Pd complexes was confirmed by increasing their absorbance after adding different concentrations of cholesterol (Fig. 10a,c). The interaction between palladium and ruthenium complexes with cholesterol was made by hydrogen bonds between the hydroxyl proton of cholesterol and the NH nitrogen of PhNHCS group, and also between the NH proton of PhNHCS group and the hydroxyl oxygen of cholesterol. Cholesterol cannot be bound to the complex by metal ion because the first coordination sphere around the central metal atom was complete.

From the calibration plots (Fig. 10b,d) and above equation ($\frac{1}{A-A_0} = \frac{1}{K\Delta\varepsilon[LM_2][chol]} + \frac{1}{\Delta\varepsilon[LM_2]_0}$), $\varepsilon\Delta$ and the formation constants (K) are calculated, and reported in table 2.

The results show that the compound formed with Ru complex exhibits higher formation constant (logK=5.4) than the one determined for Pd complex-cholesterol compound (logK=4.7), indicating that the formation of bonds between Ru complex and cholesterol is easier than the formation of bands between Pd complex and cholesterol (Pd complex is more stable than Ru complex). The interaction of the complexes with cholesterol through hydrogen bonds is confirmed by the obtained low values of formation constants of the complex-cholesterol system.

3. 8. Quenching of fluorescence and limit of detection of cholesterol

3. 8. 1. Quenching of fluorescence

The Stern-Volm oxygen er method was used to determine the quenching constants for metal complex-cholesterol systems. Fluorometric titration of both chelates with cholesterol caused a significant change in the fluorescence spectra of Pd and Ru complexes. During interaction between metal complexes and cholesterol, a fluorescence quenching has been observed. It was clearly observed that increasing the concentration of cholesterol decreases the fluorescence intensity. The cholesterol reacts with Pd and Ru complexes by reducing their fluorescence intensity.

The fluorescence emission spectra recorded at excitation absorption wavelength 290 nm (Pd complex) and 395 nm (Ru complex) showed intensities of maximum emission at 398 nm and 537 nm, respectively (Fig. 11a,c). Successive additions of cholesterol caused decrease in the intensity of fluorescence, indicating a change of the electronic structure of the metal complexes and training of LM_2-cholesterol links. This quenching may also be explained by the fact that the complex could involve an electronic transition (charge) between the complex and cholesterol.

By means of the Stern-Volmer equation, and from the slope of the calibration plot $\frac{I_0}{I} = f[chol]$ (Fig. 11b,d), the quenching constants (Ksv) were calculated and are presented in table2.

The results of fluorometric measurements in the presence of cholesterol revealed an important fluorescence quenching with Pd complex. The Stern-Volmer constant determined for Pd chelate-cholesterol (130.7 L/mol) is almost twice greater than that determined for Ru chelate (78.6 L/mol), indicating that Pd complex binds more readily with cholesterol that Ru complex. In conclusion, cholesterol interacts more easily with Pd complex than Ru complex.

3. 8. 2 Limit of detection of cholesterol

To evaluate the influence of cholesterol concentration on fluorescence intensity of the complexes, the calibration plots were reported (Fig. 11b,d), which revealed that the values of I_0/I were directly proportional to the concentrations of cholesterol from 0 to 4.76×10^{-3} M for Pd complex and 5.08×10^{-3} M for Ru complex, with a linear regression equation of $\frac{I_0}{I} = 130.7011[cholesterd] + 1.0024$ (R^2=0.994) and $\frac{I_0}{I} = 78.6365[cholesterd] + 1.0354$ (R^2=0.994), respectively.

The limit of detection of cholesterol (LOD) is calculated from the calibration plot of the fluorescence intensity of Pd and Ru complexesas versus concentration of cholesterol. The slope of the calibration plot is used to determine LOD by the following equation:

$$LOD = \frac{3s}{m}$$

Where *s* is the standard deviation of the blank signal and *m* is the slope of the calibration plot. The results (Table 3.) showed that LOD determined with Pd complex (4.6 μM) is lower (better) than LOD calculated using Ru complex (19.1 μM) and earlier reported detection

limits of cholesterol around linear range of 0-5 mM using ZnO/ZnS nano-heterostructures and ZnS nanotubes (LOD:20 μM; Linear range: 0.4-3.0 μM) [55], An upconversion nanocomposite G/Ti(G)-3DNS/CS/ChOx (LOD:6 μM; Linear range: 0.05-8.0 μM) [56], W/ferrocyanide/[ChO/ChEt] (LOD:10 μM; Linear range: 0.05-3.0 μM) [57], ChOx/AgNPs/GCE (LOD: 180 μM; Linear range: 0.28-3.3 μM) [58], Nafion/ChOx-Ppy/PB/SAM/Pt (LOD: 12 μM; Linear range: 0.05-3.0 μM) [59] and ZnO/ZnS/ChOx (LOD: 400 μM; Linear range: 0.4-4.0 μM) [60].

4. Conclusion

In this work, a novel bis-[1-(2-[(2-hydroxynaphthalen-1-yl) methylidene]amino}ethyl)-1-ethyl-3-phenylthiourea] Schiff base and its binuclear palladium and ruthenium complexes have been synthesized and characterized. These chelates were used to analysis of cholesterol by fluorometric method.

The characterization of the Pd and Ru complexes using different methods such as elemental analysis NMR, FTIR, UV-Visible, TGA and DFT, suggests a square planar around Pd metal and an octahedral environment around ruthenium.

The antioxidant activity showed that Ru complex has a significant activity (IC_{50}=3.46±0.02 μg/mL) compared to that of Pd complex (IC_{50}=13.68±0.05 μg/mL), and the antibacterial activity revealed that the activity was increased upon coordination of ligand (L) with metal ions.

The stability of the synthesized complexes showed that the complexes of palladium and ruthenium were formed at a 2:1 metal to ligand ratio, and Pd complex ($logK_s$=8.2) are more stable than Ru complex ($logK_s$=7.4). The interaction study of cholesterol with metal complexes reveals that Ru complex-cholesterol compound exhibits a higher formation constant (logK=5.4) compared to that calculated for Pd complex-cholesterol (logK=4.7).

The fluorometric measurements showed important fluorescence extinction with palladium complex, indicating a sensitive fluorometric response for the determination of cholesterol. Finally, the limit of detection of cholesterol using Pd complex (4.6 µM) was much lower than LOD determined using other published sensors around 0-5 mM cholesterol concentration range.

Acknowledgments

The authors would like to acknowledge the MESRS Algerian Ministry and Directorate-General for Scientific Research and Technological Development (Algeria) for supporting the present research.

References

[1] L.J Li, B. Fu, Y. Qiao, C. Wang, Y.Y. Huang, C.C. Liu, C. Tian, J.L. Du, Synthesis, characterization and cytotoxicity studies of platinum(II) complexes with reduced amino acid ester Schiff-bases as ligands, Inorg. Chim. Acta 419 (2014) 135–140.

[2] M.S. El-Shahawi, M.S. Al-Jahdali, A.S. Bashammakh, A.A. Al-Sibaai, H.M. Nassef Spectroscopic and electrochemical characterization of some Schiff base metal complexes containing benzoin moiety, Spectrochimica Acta Part A: Molecular and Biomolecular Spectroscopy, 113 (2013) 459-465.

[3] X. Zhang, H. Guo, F. Yang, J. Yuan, Ion complexation-controlled columnar mesophase of calix[4]arene–cholesterol derivatives with Schiff-base bridges, Tetrahedron Lett. 57 (2016) 905–909.

[4] I. Saito, K. Yamagishi, Y. Kokubo, H. Yatsuya, H. Iso, N. Sawada, M. Inoue, S. Tsugane, Association of high-density lipoprotein cholesterol concentration with different types of

stroke and coronary heart disease: The Japan Public Health Center-based prospective (JPHC) study, Atherosclerosis 265 (2017) 147-154.

[5] M. Doria, L. Maugest, G.Lizard, A. Vejux, Contribution of cholesterol and oxysterols to the pathophysiology of Parkinson's disease, Free Radical Biol. Med. 101 (2016) 393-400.

[6] J. Huang, Y. Liu, P. Zhang, Y. Li, L. Ding, A temperature-triggered fiber optic biosensor based on hydrogel-magnetic immobilized enzyme complex for sequential determination of cholesterol and glucose, J. Biochem. Eng. 125 (2017) 123–128.

[7] L.S. Eberlin, A.L. Dill, A.B. Costa, D.R. Ifa, L. Cheng, T. Masterson, M. Koch, T.L. Ratliff, R.G. Cooks, Cholesterol sulfate imaging in human prostate cancer tissue by desorption electrospray ionization mass spectrometry, Anal. Chem. 82 (2010) 3430–3434.

[8] P.M. Elias, M.L. Williams, E.H. Choi, K.R. Feingold, Role of cholesterol sulfate inepidermal structure and function: lessons from X-linked ichthyosis, BBA Mol. Cell Biol. Lipids 1841 (2014) 353–361.

[9] L.N. Zhou, Y. Liao, P.Y. Yin, Z.D. Zeng, J. Li, X. Lu, L.M. Zheng, G.W. Xu, Metabolic profiling study of early and late recurrence of hepatocellular carcinoma based on liquid chromatography–mass spectrometry, J. Chromatogr. B 966 (2014) 163–170.

[10] Z. Kejíka, M. Havlík, T. Bˇríza, R. Kaplánek, B. Dolensk´y, J. Králová, P. Martásek, V. Král, Methinium colorimetric sensors for the determination of cholesterol sulfate in an aqueous medium, Sens. Actuators B 245 (2017) 1032-1038.

[11] C.H.L. Shackleton, S. Reid, Diagnosis of recessive X-linked ichthyosis –quantitative HPLC mass-spectrometric analysis of plasma for cholesterol sulfate, Clin. Chem. 35 (1989) 1906–1910.

[12] M.P. Veares, R.P. Evershed, M.C. Prescott, L.J. Goad, Quantitative-determination of cholesterol sulfate in plasma by stable isotope-dilution fast-atom-bombardment mass-spectrometry, Biomed. Environ. Mass Spectrom. 19 (1990) 583–588.

[13] F.A.J. Muskiet, G. Jansen, B.G. Wolthers, A. Marinkovicilsen, P.C.V. Vader, Gas-chromatographic determination of cholesterol sulfate in plasma and erythrocytes, for the diagnosis of recessive X-linked ichthyosis, Clin. Chem. 29 (1983) 1404–1407.

[14] S. Serizawa, T. Nagai, Y. Sato, Simplified method of determination of serum-cholesterol sulfate by reverse phase thin-layer chromatography, J. Invest. Dermatol. 89 (1987) 580–587.

[15] P.R. Solanki, A. Kaushik , A.A. Ansari, B.D. Malhotra, Nanostructured zinc oxide platform for cholesterol sensor. Appl. Phys. Lett. 94 (2009) 143901.

[16] N. Joshi, K. Rawat, P.R Solanki, H.B. Bohidar, Enzyme-free and biocompatible nanocomposite based cholesterol sensor, J. Biochem. Eng. 102 (2015) 69–73.

[17] X. Lina, Y. Nia, S. Kokot, Electrochemical cholesterol sensor based on cholesterol oxidase and MoS2-AuNPs modified glassy carbon electrode, Sens. Actuators B 233 (2016) 100–106.

[18] H. Yang, L. Li, Y. Ding, D. Ye, Y. Wang, S. Cui, L. Liao, Molecularly imprinted electrochemical sensor based on bioinspired Au microflowers for ultra-trace cholesterol assay, Biosens. Bioelectron. 92 (2017) 748–754.

[19] V. Sharma, S.M. Mobin, Cytocompatible peroxidase mimic CuO:graphene nanosphere composite as colorimetric dual sensor for hydrogen peroxide and cholesterol with its logic gate implementation, Sens. Actuators B 240 (2017) 338–348.

[20] M. Chebl, Z. Moussa, M. Peurla, D. Patra, Polyelectrolyte mediated nano hybrid particle as a nano-sensor with outstandingly amplified specificity and sensitivity for enzyme free estimation of cholesterol, Talanta 169 (2017) 104–114.

[21] X.T Sun, Y. Zhang, D.H Zheng, S. Yue, C.G Yang, Z.R Xu, Multitarget sensing of glucose and cholesterol based on Janus hydrogel microparticles, Biosens. Bioelectron. 92 (2017) 81–86.

[22] N. Gupta, D. Singhal, A.K. Singh, N. Singh, U.P. Singh, A highly selective chromogenic sensor for Mn^{2+}, turn-off fluorometric for Hg^{2+} ion, and turn-on fluorogenic sensor for F^{-} ion with the practical application, Spectrochim. Acta, Part A 176 (2017) 38–46.

[23] Q. Sun, S. Fang, Y. Fang, Z. Qian, H. Feng, Fluorometric detection of cholesterol based on β-cyclodextrin functionalized carbon quantum dots via competitive host-guest recognition, Talanta 167 (2017) 513–519.

[24] A. Rauf, A. Shah, A.A Khan, A.H. Shah, R. Abbasi, I.Z Qureshi, S. Ali, Synthesis, pH dependent photometric and electrochemical investigation, redox mechanism and biological applications of novel Schiff base and its metallic derivatives, Spectrochim. Acta, Part A 176 (2017) 155–167.

[25] Y. Huang, L. Cui, Y. Xue, S. Zhang, G. Li, Ultrasensitive cholesterol biosensor based on enzymatic silver deposition on gold nanoparticles modified screen-printed carbon electrode, Mater. Sci. Eng. C 77 (2017) 1-8.

[26] N.R. Nirala, P.S. Saxena, A. Srivastava, Colorimetric detection of cholesterol based on enzyme modified gold nanoparticles, Spectrochim. Acta, Part A 190 (2018)506-512.

[27] S. Nantaphol, O. Chailapakul, W. Siangproh, Sensitive and selective electrochemical sensor using silver nanoparticles modified glassy carbon electrode for determination of cholesterol in bovine serum, Sens. Actuators B 207 (2015) 193–198.

[28] N.R. Nirala, S. Abraham, V. Kumar, A. Bansal, A. Srivastava, P.S. Saxena, Colorimetric detection of cholesterol based on highly efficient peroxidase mimetic activity of graphene quantum dots, Sens. Actuators B 218 (2015) 42–50.

[29] M.H. Zhang, R. Yuan, Y.Q. Chai, C. Wang, X.P. Wu, Cerium oxide–graphene as the matrix for cholesterol sensor, Anal. Biochem. 436 (2013) 69–74.

[30] S. Komathi, N. Muthichamy, K.P. Lee, A.I. Gopalan, Fabrication of a novel dual mode cholesterol biosensor using titanium dioxide nanowire bridged 3D grapheme nanostacks, Biosens. Bioelectron. 84 (2016) 64–71.

[31] W.H Chiang, P.Y Chen, P.C Nien, K.C Ho, Amperometric detection of cholesterol using an indirect electrochemical oxidation method, Steroids 76 (2011) 1535–1540.

[32] J. Singh, P. Kalita, M.K. Singh, B.D. Malhotra, Nanostructured nickel oxide– chitosan film for application to cholesterol sensor. Appl. Phys. Lett. 98 (2011) 123702.

[33] A. Umar, R. Ahmad, R. Kumar, A.A. Ibrahim, S. Baskoutas, $Bi_2O_2CO_3$ nanoplates: fabrication and characterization of highly sensitive and selective cholesterol biosensor, J. Alloys Compd. 683 (2016) 433–438.

[34] S. Gilbert, H. Kyung Jeong, P.A. Dowben, Cyclodextrin-carbon nanotube composites for fluorescent detection of cholesterol, Chem. Phys. Lett. (2017), doi:10.1016/j.cplett. 2017.09.024

[35] S. Pakapongpan, A. Tuantranont, P. Sritongkham, Cholesterol biosensor based on direct electron transfer of cholesterol oxidase on multi-wall carbon nanotubes, Biomed. Eng. Int. Conf. (2011) 138–141.

[36] W. Liu, H. Yang, C. Ma, Y. Ding, S. Ge, J. Yu, M. Yan, Graphene—palladium nanowires based electrochemical sensor using $ZnFe_2O_4$—graphene quantum dots as an effective peroxidase mimic, Anal. Chim. Acta 852 (2014) 181–188.

[37] B. Bajaj, H.I. Joh, S.M. Jo, G. Kaur, A. Sharma, M. Tomar, V. Gupta, S. Lee, Controllable one step copper coating on carbon nanofibers for flexible cholesterol biosensor substrates, J. Mater. Chem. B 2 (2016) 229–236.

[38] National Committee for Clinical Laboratory Standards, Methods for dilution antimicrobial susceptibility tests for bacteria that grow aerobically. Approved standard *In* NCCLS document M7-A4, 4th ed. National Committee for Clinical Laboratory Standards,

Wayne, Pa., 1997.

[39] K. Nakamoto, Infrared and Raman Spectra of Inorganic and Coordination Compounds, Wiley-Interscience, New York, 1986.

[40] A. Prakash, B. Singh, N. Bhojak, D. Adhikari, Synthesis and characterization of bioactive zinc(II) and cadmium(II) complexes with new Schiff bases derived from 4-nitrobenzaldehyde and acetophenone with ethylenediamine, Spectrochim. Acta A 76 (2010) 356–362.

[41] V. Klimesova, J. Koci, K. Waisser, J. Kaustova, New benzimidazole derivatives as antimycobacterial agents, Farmaco 57 (2002) 259-265.

[42] B.T. Khan, S.M. Zakeeruddin, Platinum(II) and palladium(II) complexes with substituted pyrimidines, Trans. Met. Chem.16 (1991) 119-121.

[43] P. Kalaivani, R. Prabhakaran, M.V. Kaveri, R. Huang, R.J. Staples, K. Natarajan, Synthesis, spectral, X-ray crystallography, electrochemistry, DNA/protein binding and radical scavenging activity of new palladium (II) complexes containing triphenylarsine, Inorg. Chem. Acta 405 (2013) 415-426.

[44] M.M.T. Khan, D. Srinivas, R.I. Khureshy, N.H. Khan, Synthesis, characterization, and EPR studies of stable ruthenium(III) Schiff base chloro and carbonyl complexes, Inorg. Chem. 29 (1990) 2320–2326.

[45] M.M. Subarkhan, R. Ramesh, Binuclear ruthenium(III) bis(thiosemicarbazone) complexes: Synthesis, spectral, electrochemical studies and catalytic oxidation of alcohol, Spectrochim. Acta A 138 (2015) 264–270.

[46] H. Repich, S. Orysyk, V. Bon, P. Savytskyi, V. Pekhnyo, Mono- and binuclear Pd(II) complexes with 2-(5,6-dimethyl-4-oxo-3,4-dihydrothieno[2,3-d]pyrimidin-2-yl)-N-phenylhydrazinecarbothioamide: Synthesis, crystal structure and spectroscopic characterization, J. Mol. Struct. 1102 (2015) 161-169.

[47] A.B. Lever, Inorganic Electronic Spectroscopy, second ed., Elsevier, Amstterdam, 1982. pp. 544–552.

[48] S. Konar, A. Jana, K. Das, S. Ray, S. Chatterjee, J.A. Golen, A.L. Rheingold, S.K. Kar, Synthesis, crystal structure, spectroscopic and photoluminescence studies of manganese(II), cobalt(II), cadmium(II), zinc(II) and copper(II) complexes with a pyrazole derived Schiff base ligand, Polyhedron 30 (2011) 2801-2808.

[49] V. Govindaraj, S. Ramanathan, Synthesis, spectral characterization, electrochemical, and fluorescence studies of biologically active novel Schiff base complexes derived from E-4-(2 hydroxy-3-methoxybenzylideneamino)-N-(pyrimidin-2-yl)benzenesulfonamide, Turkish J. Chem. 38 (2014) 521-530.

[50] Y. Zhao, D.G. Truhlar, The M06 suite of density functionals for main group thermochemistry, thermochemical kinetics, noncovalent interactions, excited states, and transition elements: two new functionals and systematic testing of four M06-class functionals and 12 other functionals, Theor. Chem. Acc. 120 (2008) 215–241.

[51] P.J. Hay, W.R. Wadt, Ab initio effective core potentials for molecular calculations. Potentials for the transition metal atoms Sc to Hg, J. Chem. Phys. 82 (1985) 270–283.

[52] M.J. Frisch, G.W. Trucks, H.B. Schlegel, G.E. Scuseria, M.A. Robb, J.R. Cheeseman, J.A. Montgomery, T. Vreven, K.N. Kudin, J.C. Burant, J.M. Millam, S.S. Iyengar, J. Tomasi, V. Barone, B. Mennucci, M. Cossi, G. Scalmani, N. Rega, G.A. Petersson, H. Nakatsuji, M. Hada, M. Ehara, K. Toyota, R. Fukuda, J. Hasegawa, M. Ishida, T. Nakajima, Y. Honda, O. Kitao, H. Nakai, M. Klene, X. Li, J.E. Knox, H.P. Hratchian, J.B. Cross, C. Adamo, J. Jaramillo, R. Gomperts, R.E. Stratmann, O. Yazyev, A.J. Austin, R. Cammi, C. Pomelli, J.W. Ochterski, P.Y. Ayala, K. Morokuma, G.A. Voth, P. Salvador, J.J. Dannenberg, V.G. Zakrzewski, S. Dapprich, A.D. Daniels, M.C. Strain, O. Farkas, D.K. Malick, A.D. Rabuck, K. Raghavachari, J.B. Foresman, J.V.

Ortiz, Q. Cui, A.G. Baboul, S. Clifford, J. Cioslowski, B.B. Stefanov, G. Liu, A. Liashenko, P. Piskorz, I. Komaromi, R.L. Martin, D.J. Fox, T. Keith, M.A. Al-Laham, C.Y. Peng, A. Nanayakkara, M. Challacombe, P.M.W. Gill, B. Johnson, W. Chen, M.W. Wong, C. Gonzalez, J.A. Pople, Gaussian 03, Revision A.1, Gaussian Inc., Pittsburgh PA, 2003.

[53] H. Miller, F. Rigelhof, L. Marquart, M. Kanter, Antioxidant content of whole grain breakfast cereals, fruits and vegetables, J. Am. Coll. Nut. 19 (2000) 312-319.

[54] G.G.Mohamed, F.A. Nour-EI Dien, E.A. El-Gamel, Thermal Behaviour of Metal Complexes of 6-(2-Pyridylazo)-3-acetamidophenol, J. Therm. Anal. Cal., 67 (2002) 135-149.

[55] A.K. Giri, C. Charan, S.C. Ghosh, V.K. Shahi, A.B. Panda, Phase and composition selective superior cholesterol sensing performance of ZnO/ZnS nano-heterostructure and ZnS nanotubes, Sens. Actuators B 229 (2016) 14-24.

[56] Y. Ding, H. Zhu, X. Zhang, J.Gao, E.S. Abdel- Halim, L. Jiang, J.-J. Zhu, An upconversion nanocomposite for fluorescence resonance energy transfer based cholesterol-sensing in human serum, Nanoscale 6 (2014) 14792-14798.

[57] A. Huang, Y. An, L. Tang, X. Jiang, H. Chen, W. Bi, Z. Wang, W. Zhang, A dual enzymatic-biosensor for simultaneous determination of glucose and cholesterol in serum and peritoneral macrophases of diabetic mice: evaluation of the diabetes-accelerated atherosclerosis risk, Anal. Chim. Acta 707 (2011) 135-141.

[58] B.C. Ozer, H. Ozyoruk, S.S. Celebi, A. Yildyz, Amperometric enzyme electrode for free cholesterol determination prepared with cholesterol oxidase immobilized in poly(vinylferrocenium) film, Enzyme Microb. Technol. 40 (2007) 262-265.

[59] A.A. Ansari, A. Kaushik, P.R. Solanki, B.D. Malhotra, Electrochemical cholesterol sensor based on tin oxide-chitosan nanobiocomposite film, Electroanalysis 21 (2009) 965-972.

[60] J.C. Vidal, J. Espuelas, E. Garcia-Ruiz, J.R. Castillo, Amperometric cholesterol biosensors based on the electropolymerization of pyrrole and the electrocatalytic effet of prussian-blue layers helped with self-assembled monolayers, Talanta 64 (2004) 655-664.

Table 1. Energetic properties, dipole moments, energies of HOMO, LUMO orbitals and energy gap of the different forms of palladium and ruthenium complexes.

Parameters /geometry forms	Relative energy (ΔE: kcal/mol)	Dipole moment (Deby)	HOMO (a.u)	LUMO (a.u.)	ΔE (eV)
Ru complex					
Form1	-2324.73	8.19	-5.12	-4.52	0.60
Form2	-2234.20	5.18	-4.13	-3.69	0.44
Form3	-2269.08	9.82	-4.38	-3.74	0.64
Form4	-2521.18	17.03	-4.49	-3.11	1.38
Form5	-2339.91	8.27	-4.83	-3.83	1.00
Form6	-2441.08	18.02	-4.15	-3.31	0.84
Pd complex					
Form1	-2264.96	5.10	-3.14	-2.13	1.01
Form2	-2262.61	4.85	-3.29	-2.64	0.65
Form3	-2263.89	7.75	-3.42	-2.94	0.48
Form4	-2405.66	12.25	-4.76	-3.40	1.36
Form5	-2369.66	7.75	-4.13	-2.97	1.16
Form6	-2400.37	14.22	-3.18	-2.88	0.93

Table 2. Stability Constants of complexes, formation constants of complex-cholesterol compounds, values of Δε, Stern-volmer constants and limit of detection calculated by spectrophotometry and fluorescence techniques.

Complexes	Ru complex	Pd complex	Ru complex-cholesterol	Pd complex-cholesterol
K (L/mol)	2.955×10^{7}	1.571×10^{8}	2.405×10^{5}	5.062×10^{4}
logK (L/mol)	7.4	8.2	5.4	4.7
Δε	-	-	106.5	110.0
K_{SV} (L/mol)	-	-	78.6	130.7

Table 3. Determination of cholesterol by different sensors.

Materials	Linear range (mM)	LOD (μM)	References
ZnO/ZnS	0.4–3.0	20	[52]
G/Ti(G)-3DNS/CS/ChOx	0.05–8.0	6	[53]
W/ferrocyanide/[ChO/ChEt]	0.05–3.0	10	[54]
ChOx/AgNPs/GCE	0.28–3.3	180	[55]
Nafion/ChOx-Ppy/PB/SAM/Pt	0.05–3.0	12	[56]
ZnO@ZnS/ChOx	0.4–4.0	400	[57]
Pd complex ($C_{42}H_{38}N_6O_2S_2Cl_2Pd_2$,$2H_2O$)	0-4.76	4.6	This work
Ru complex ($C_{42}H_{42}N_6O_4S_2Cl_4Ru_2$,$4H_2O$)	0-5.08	19.1	This work

Figure captions

Fig 1. FT-IR spectra of compounds: (a) L; (b) Ru complex; (c) Pd complex.

Fig. 2. Nuclear magnetic resonance spectra of L and metal complexes in $DMSO_{d6}$: (a) ^{1}H-^{13}C HSQC-NMR of L; (b) ^{1}H-^{13}C HSQC-NMR of Ru complex; (c) ^{1}H-NMR of Pd complex.

Fig. 3. UV-Visible spectra of the compounds in DMSO: (a_1) L (10^{-5} M); (a_2) Pd complex (10^{-4} M); (a_3) Ru complex (10^{-4} M); (b) Ru complex (10^{-3} M), ℓ=1cm.

Fig. 4. Fluorescence spectra of L and metal complexes.

Fig. 5. TGA spectra of metal complexes.

Fig. 6. Geometry forms and Frontier molecular orbitals of the complexes: (a) form 4 of Pd complex; (d) form 4 of Ru complex; (b) HOMO of form 4 of Pd complex; (e) HOMO of form 4 of Ru complex; (c) LUMO of form 4 of Pd complex; (f) LUMO of form 4 of Ru complex.

Fig. 7. Cyclic voltammograms of L and metal complexes in DMSO and TBAP (10^{-2} M); Scan rate=20 mV/s.

Fig. 8. (a) Graphical representation of % antioxidant of metal complexes; (b) Antibacterial activities of L and metal complexes.

Fig. 9. (a) Spectrophotometric titration curves of L ($1{,}73.10^{-4}$M) with Ru^{3+} (0.01 M); (b) Plot of $1/(A-A_0)$ vs. $(1/[Ru^{3+}]^2)$; (c) Plot of $1/(A-A_0)$ vs. $(1/[Pd^{2+}]^2)$.

Fig. 10. Spectrophotometric titration of: (a) and (b) Ru complex and (c) and (d) Pd complex with cholesterol (0.01 M).

Fig. 11. Fluorometric titration of metal complexes with cholesterol (0.01 M) and Stern-Volmer plot: (a) and (b) Pd complex (λ_{ex}=290 nm); (c) and (d) Ru complex (λ_{ex}=395 nm).

Fig. 1S. ATR spectra of the compounds: (a) L; (b) Ru complex; (c) Pd complex.

Fig. 2S. Nuclear magnetic resonance spectra of the compounds in $DMSO_{d6}$: (a) ^{1}H-NMR of L; (b) Cosy-NMR of L; (c) ^{13}C-NMR of Ru complex.

Fig. 3S. EDS analysis of metal complexes formed with L.

Fig. 4S. Cyclic voltammograms of (a) Ru complex and (c) Pd complex performed in DMSO and TBAP (10^{-2} M) at different scan rates; (b) Oxidation peak current vs. scan rate for Ru complex and (d) Oxidation peak current vs. scan rate for Pd complex.

Fig. 5S. Spectrophotometric titration curves of L ($1{,}73.10^{-4}$M) with Pd^{2+}(0.01 M).

Scheme 1. Synthetic route of ligand (L).

Scheme 2. Synthetic route of Pd and Ru complexes.

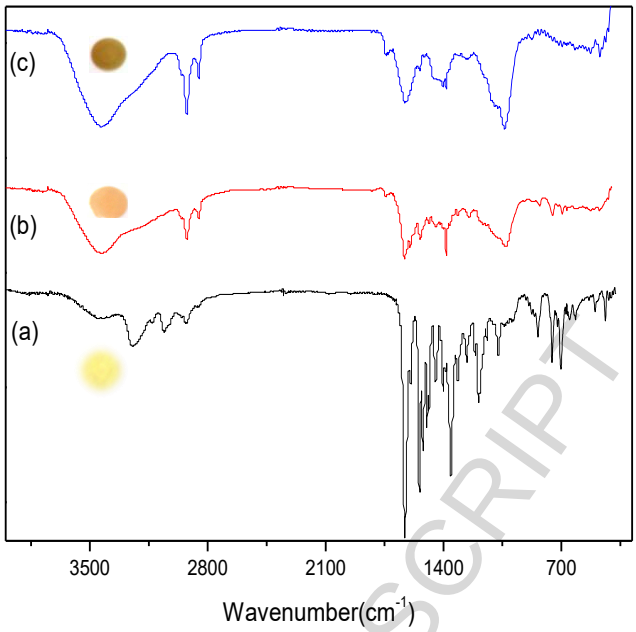

Fig 1.

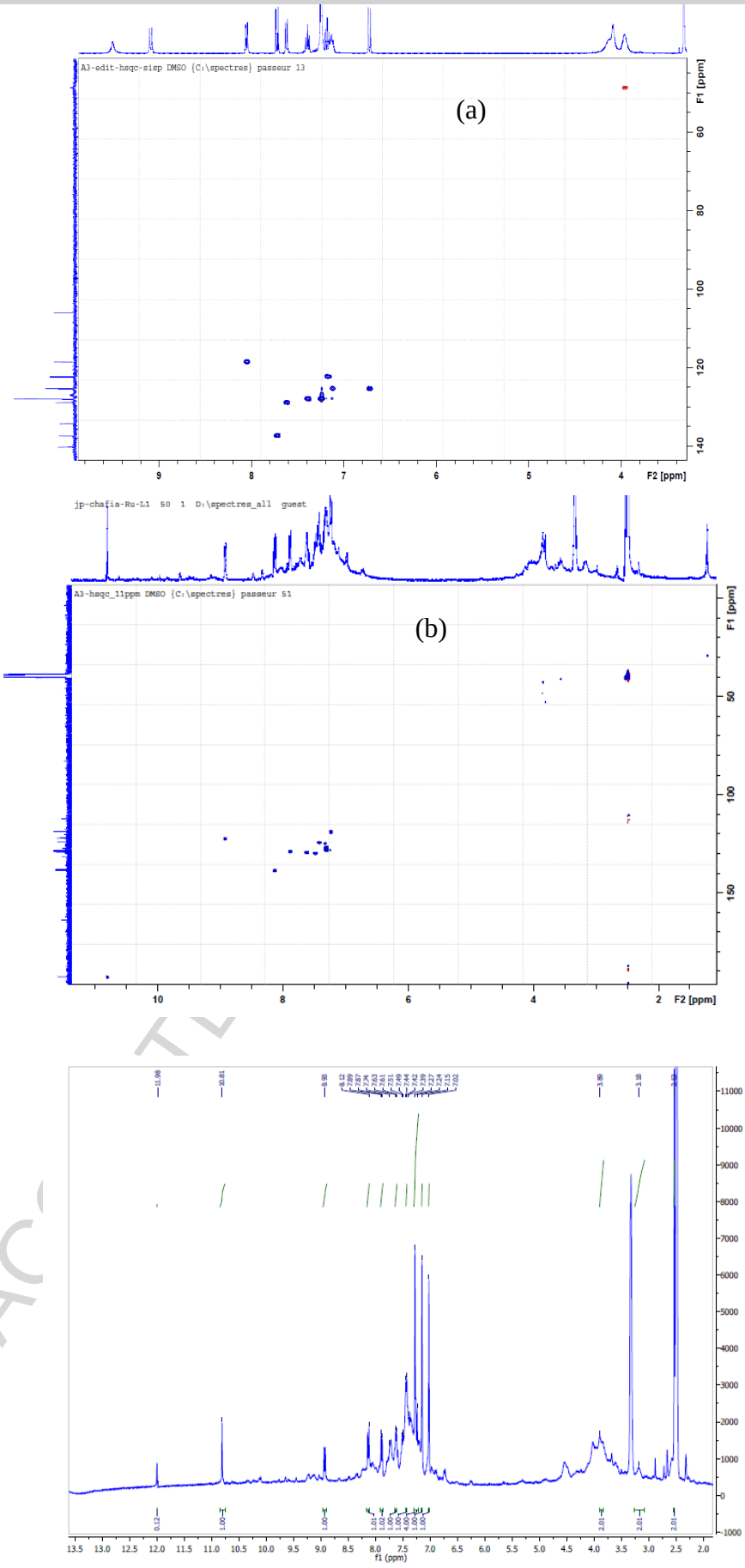

Fig. 2.

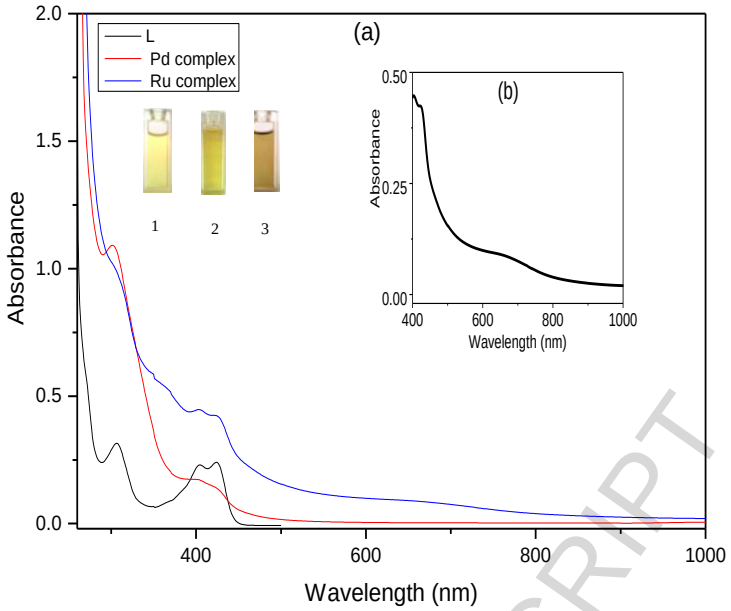

Fig. 3.

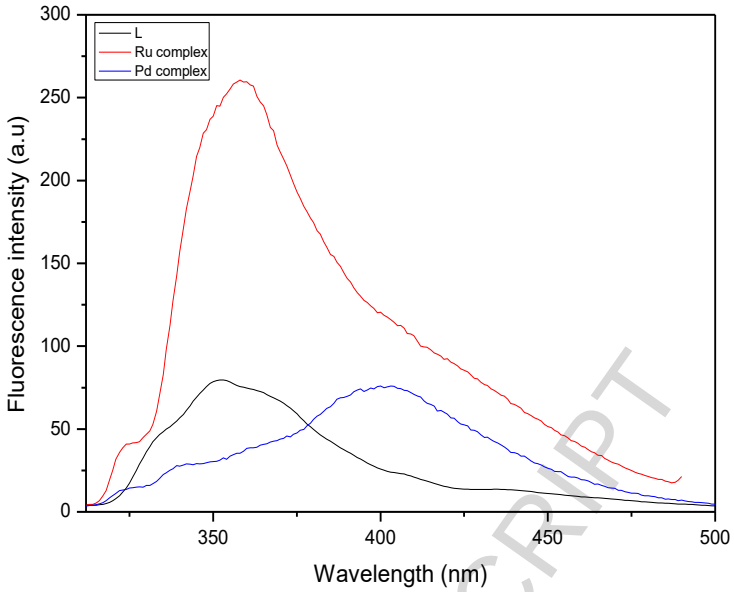

Fig. 4.

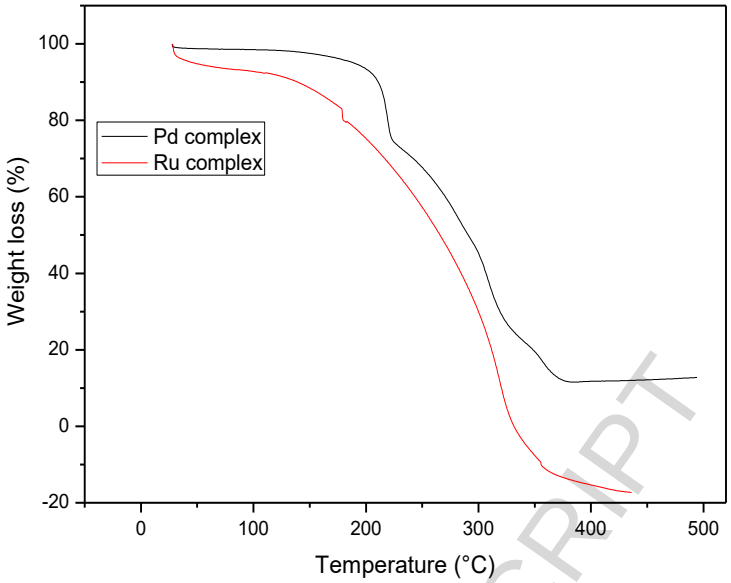

Fig. 5.

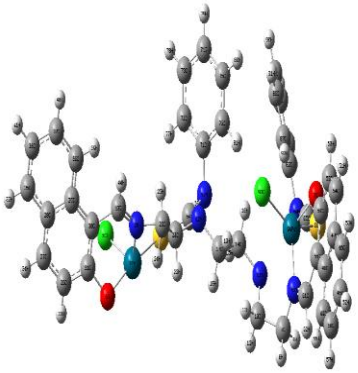

(a)

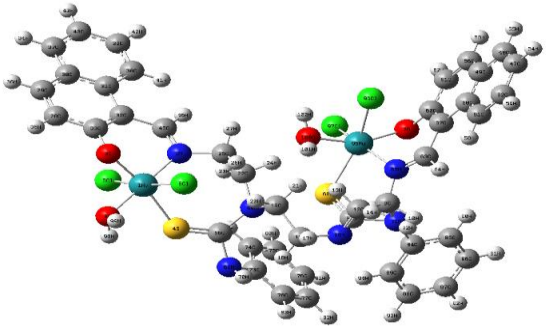

(d)

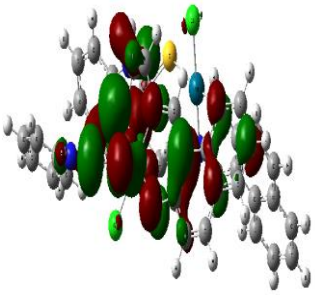

(b)

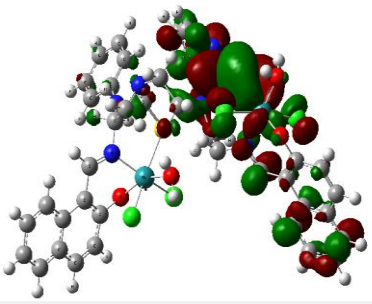

(e)

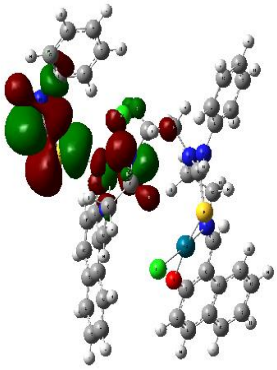

(c)

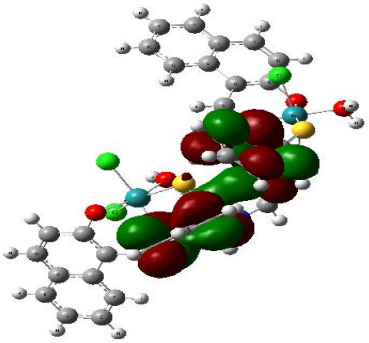

(f)

Fig. 6.

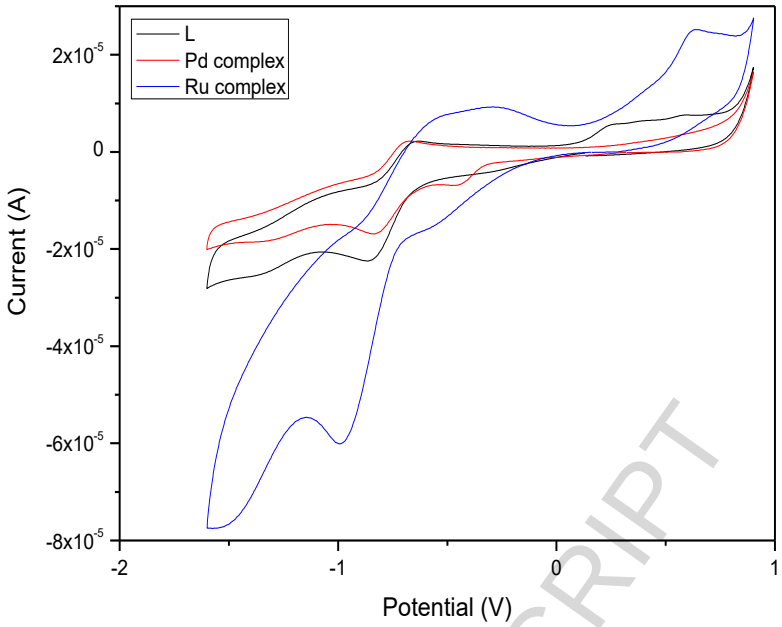

Fig. 7.

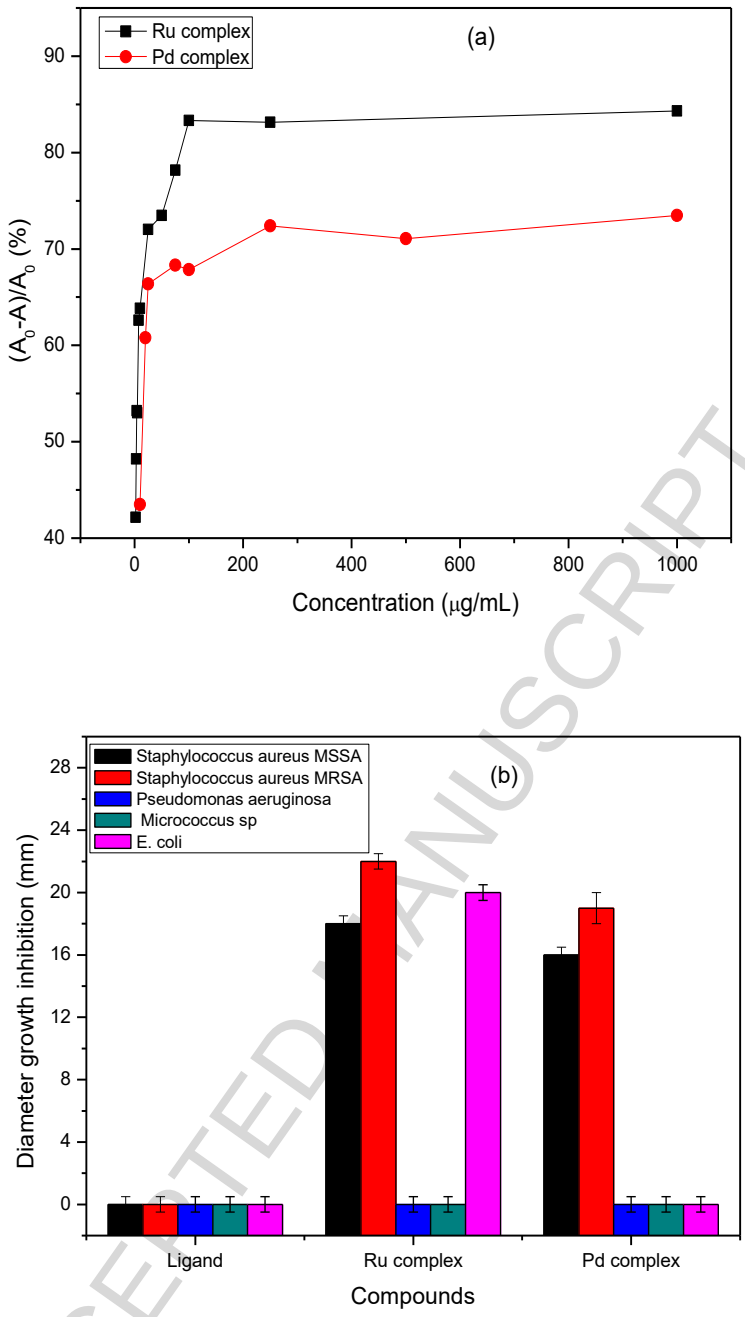

Fig. 8.

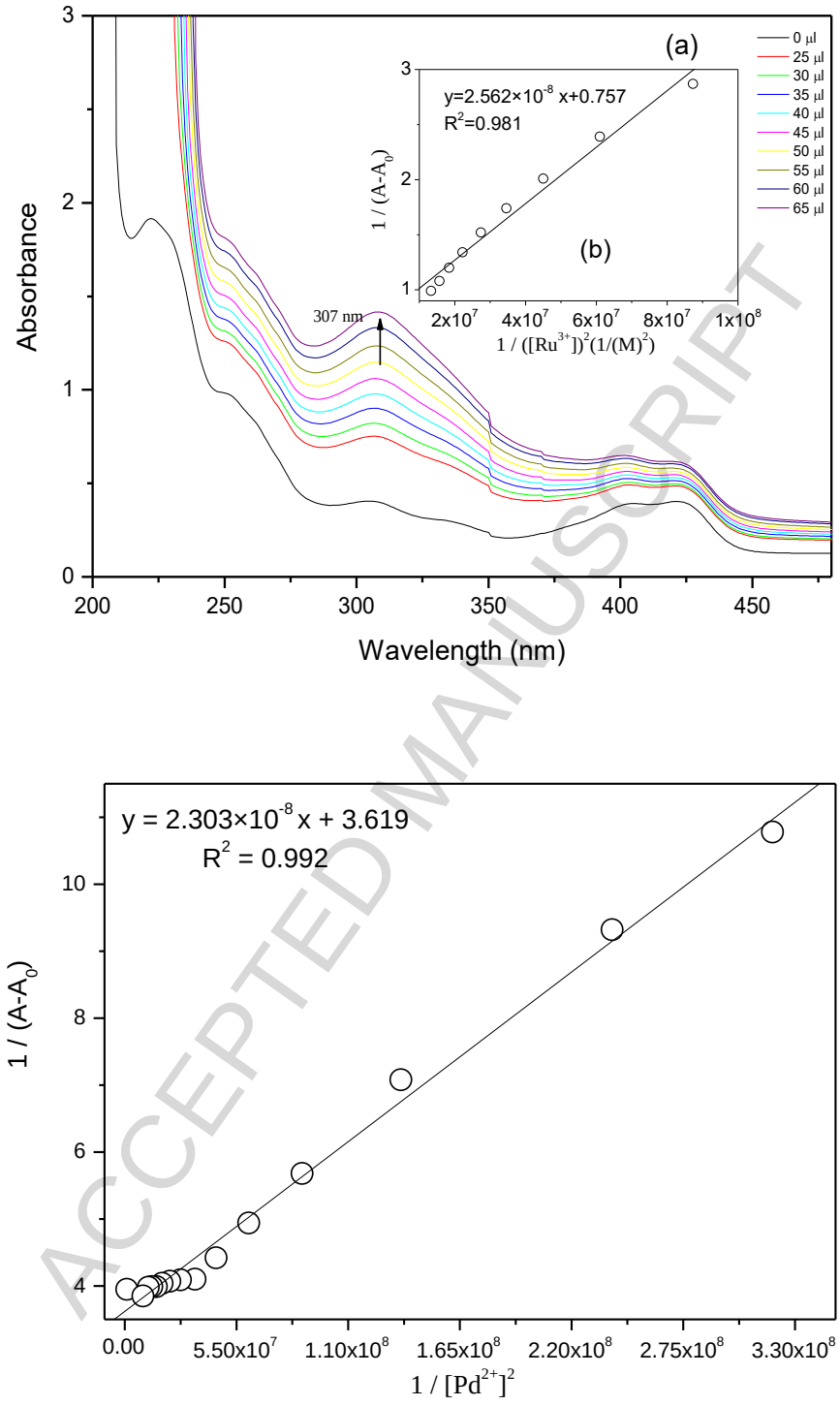

Fig. 9.

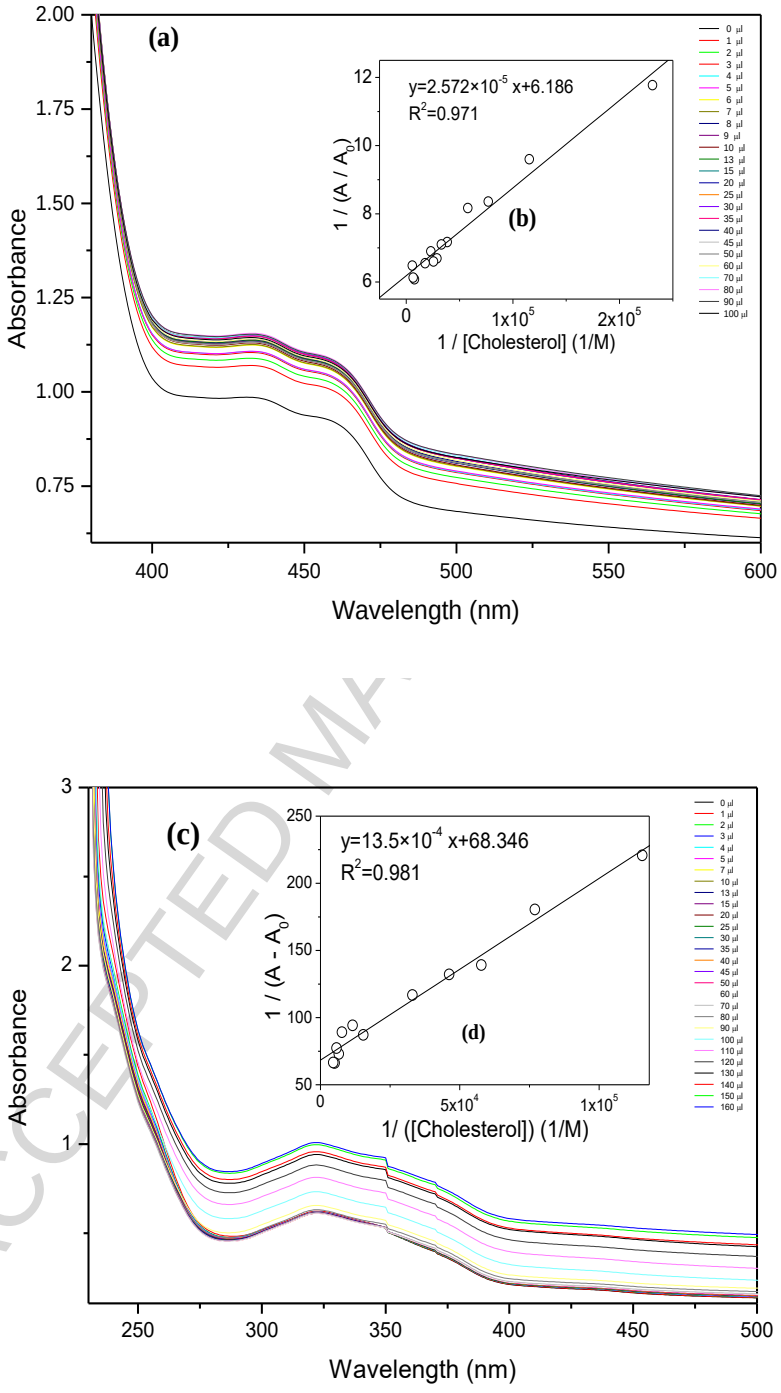

Fig. 10.

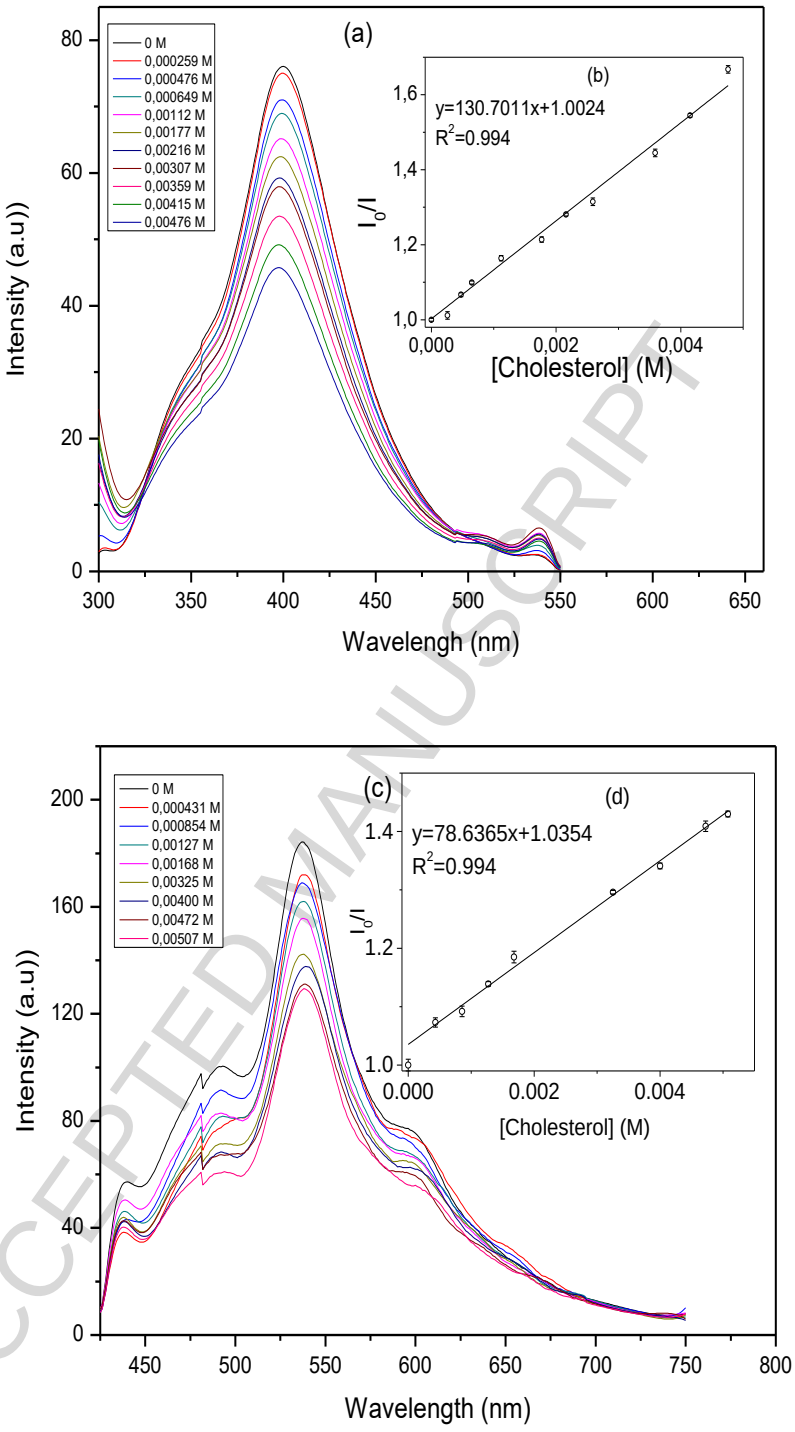

Fig. 11.

Graphical abstract

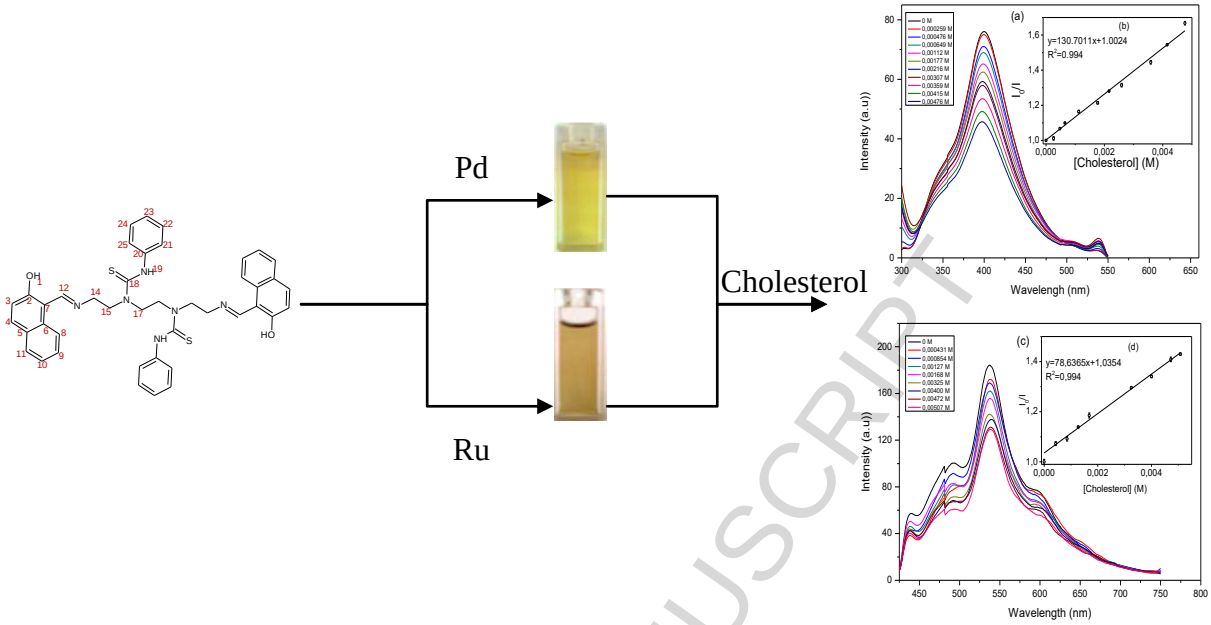

Highlights

- Novel bis-[1-(2-[(2-hydroxynaphthalen-1-yl)methylidene]amino}ethyl)-1-ethyl-3-phenylthiourea] ligand (Schiff base) and its binuclear Pd and Ru complexes were prepared and characterized.
- Stability constants of metal complexes of platinum group metals (Pd and Ru complexes) and their interaction with cholesterol were investigated using spectrophotometric method.
- Antioxidant and antibacterial activities were studied, and showed that these activities were increased upon coordination of ligand (L) with metal ions.
- Interaction study of cholesterol with Pd and Ru complexes was investigated using fluorometric technique. Ru complex-cholesterol compound exhibits the highest formation constant.
- The palladium complex formed with ligand (L) is a suitable material for the determination of cholesterol in a wide range of concentrations by using fluorescence method.